STATISTICAL PHYSICS APPROACH TO UNDERSTANDING THE MULTISCALE DYNAMICS OF EARTHQUAKE FAULT SYSTEMS

John B. Rundle,[1,2,3,4,5] Donald L. Turcotte,[4] Robert Shcherbakov,[1,2] William Klein,[6,7] and Charles Sammis[8]

Received 28 April 2003; revised 21 July 2003; accepted 6 August 2003; published 18 December 2003.

[1] Earthquakes and the faults upon which they occur interact over a wide range of spatial and temporal scales. In addition, many aspects of regional seismicity appear to be stochastic both in space and time. However, within this complexity, there is considerable self-organization. We argue that the occurrence of earthquakes is a problem that can be attacked using the fundamentals of statistical physics. Concepts of statistical physics associated with phase changes and critical points have been successfully applied to a variety of cellular automata models. Examples include sandpile models, forest fire models, and, particularly, slider block models. These models exhibit avalanche behavior very similar to observed seismicity. A fundamental question is whether variations in seismicity can be used to successfully forecast the occurrence of earthquakes. Several attempts have been made to utilize precursory seismic activation and quiescence to make earthquake forecasts, some of which show promise. *INDEX TERMS:* 3220 Mathematical Geophysics: Nonlinear dynamics; 3210 Mathematical Geophysics: Modeling; 3250 Mathematical Geophysics: Fractals and multifractals; 7209 Seismology: Earthquake dynamics and mechanics; 7260 Seismology: Theory and modeling; *KEYWORDS:* earthquakes, critical phenomena, self-organization, forecasting

Citation: Rundle, J. B., D. L. Turcotte, R. Shcherbakov, W. Klein, and C. Sammis, Statistical physics approach to understanding the multiscale dynamics of earthquake fault systems, *Rev. Geophys., 41*(4), 1019, doi:10.1029/2003RG000135, 2003.

1. INTRODUCTION: THE PROBLEM OF EARTHQUAKES

[2] Earthquakes have great scientific, societal, and economic significance. During the first 2 months of 2001 the 13 January magnitude 7.6 El Salvador earthquake, the 26 January magnitude 7.9 Gujarat, India, earthquake, and the 28 February magnitude 6.8 Seattle, Washington, United States, earthquake killed thousands of persons and caused billions of dollars in property losses. The 16 January 1995 Kobe, Japan, earthquake was only a magnitude 6.9 event and yet produced an estimated $200 billion loss. Similar scenarios are possible at any time in Los Angeles, San Francisco, Seattle, and other U.S. urban centers along the Pacific plate boundary. The magnitude of the potential loss of life and property is so great that reliable earthquake forecasting has been a long-sought-for goal. Many millions of dollars and many thousands of work years have been spent on observational programs searching for reliable precursory phenomena.

[3] Possible precursory phenomena include changes in seismicity, changes in seismic velocities, tilt and strain precursors, electromagnetic signals, hydrologic phenomena, and chemical emissions [*Turcotte*, 1991; *Scholz*, 2002]. A few successes have been reported, but, to date, no precursors to large earthquake have been detected that would provide reliable forecasts (*Nature* Debates, Debate on earthquake forecasting, http://www.nature.com/nature/debates/earthquake/, 1999, hereinafter referred to as *Nature* Debates, 1999).

[4] In terms of data acquisition several major approaches are currently being emphasized. These include (1) paleoseismic observations of historic earthquakes whose occurrence and locations are preserved in offset surficial sediments; (2) patterns of seismicity (origin time, location, and magnitude of earthquakes); (3) sur-

[1]Center for Computational Science and Engineering, University of California, Davis, California, USA.
[2]Department of Physics, University of California, Davis, California, USA.
[3]Department of Civil and Environmental Engineering, University of California, Davis, California, USA.
[4]Department of Geology, University of California, Davis, California, USA.
[5]Earth and Space Sciences Division, Jet Propulsion Laboratory, Pasadena, California, USA.
[6]Department of Physics, Boston University, Boston, Massachusetts, USA.
[7]Temporarily at Los Alamos National Laboratory, Los Alamos, New Mexico, USA.
[8]Department of Geology and Geophysics, University of Southern California, Los Angeles, California, USA.

8755-1209/03/2003RG000135*$15.00* doi:10.1029/2003RG000135

face deformation measured via Global Positioning System (GPS) networks such as the Southern California Integrated GPS Network (available at http://www.scign.org) and the Bay Area Regional Deformation network (Southern California Seismographic Network (SCSN) catalog, available from Southern California Earthquake Center (SCEC) Data Center, University of Southern California, Los Angeles, and *Nature* Debates, 1999); and (4) synthetic aperture radar interferometry (InSAR) observations of surface displacement. Observations of these data types are also planned as part of the National Science Foundation Earthscope initiative (see http://www.earthscope.org). In fact, the Plate Boundary Observatory (PBO) plans to place more than a thousand GPS, strain meter, and deformation sensors along the active plate boundary of the western coast of the United States, Mexico, and Canada at an eventual cost in excess of $100 million (*Nature* Debates, 1999).

[5] It is clearly a very high priority to utilize this wealth of new data to better understand the fundamentals of earthquake occurrence. This understanding can improve several aspects of the earthquake hazard: (1) risk assessment, determining the probability of the occurrence of an earthquake of a specified magnitude in a specified area within a specified time window, and (2) earthquake forecasting (prediction), finding patterns of behavior that can provide statistically acceptable forecasts of future major earthquakes. There are two serious limitations to a purely observational approach to the problems of understanding earthquake physics and earthquake forecasting: (1) fundamentally unobservable dynamics and (2) a vast range of space and timescales.

1.1. Unobservable Dynamics

[6] Earthquake faults occur in topologically complex, multiscale networks or systems that are driven to failure by external forces arising from plate tectonic motions [*Turcotte*, 1997; *Ben-Zion and Sammis*, 2003]. The basic problem is that the details of the true space-time, force-displacement dynamics are unobservable, in general, except in a few selected locations such as deep drill holes (Earthscope, National Science Foundation Earthscope Initiative and PBO, www.earthscope.org/, 2002) or in a very crude, time-averaged sense such as the World Stress Map [*Zoback*, 1992]. In order to completely specify the problem the true dynamics would have to be observable for all space and at all times. In fault systems these unobservable dynamics are usually encoded [*Stein*, 1999] in the time evolution of the Coulomb failure function, CFF($\mathbf{x}$, t):

$$\mathrm{CFF}(\mathbf{x}, t) \equiv \tau(\mathbf{x}, t) - \mu_s \, \sigma_N(\mathbf{x}, t) \ , \qquad (1)$$

where $\tau(\mathbf{x}, t)$ is shear stress at point $\mathbf{x}$ and time t, μ_s is the coefficient of static friction, and $\sigma_N(\mathbf{x}, t)$ is normal stress. However, the space-time patterns associated with the time, location, and magnitude of the sudden events (earthquakes) are observable, leading to a focus on understanding their observable, multiscale, apparent dynamics [*Ball*, 1999; *Eneva and Ben-Zion*, 1997a, 1997b; *Fukunaga*, 1990; *Giering and Kaminski*, 1998; *Holmes et al.*, 1996; *Lermusiaux and Robinson*, 1999; *Miller et al.*, 1999; *Molchan and Kagan*, 1992; *Mora*, 1999; *Matsu'ura et al.*, 2001; *Nijhout et al.*, 1997; *Preisendorfer and Mobley*, 1988; *Rundle et al.*, 1999, 2000b, 2000c, 2000d, 2001, 2002; *Tiampo et al.*, 2000, 2002b].

1.2. Range of Scales

[7] The second problem, equally serious, is that the nonlinear earthquake dynamics is strongly coupled across a vast range of space and timescales that are much larger than "human" dimensions [*Anghel et al.*, 2003; *Bufe and Varnes*, 1993; *Main*, 1996; *Mora*, 1999; *Rundle et al.*, 1999, 2002; *Scholz*, 2002; *Turcotte*, 1997]. Important spatial scales range from the microscopic scale (1μm to 1 cm) associated with friction to the tectonic plate boundary scale (10^3–10^4 km) associated with the driving force. These scales are summarized in Table 1 along with the relevant physics, the input from smaller scales, the output to larger scales, and relevant computational methods. Important temporal scales range from seconds (during dynamic rupture) to 10^3–10^4 years (repeat times for earthquakes) to 10^7–10^8 years (evolution of plate boundaries).

[8] Research should be focused on understanding the origins and implications of space-time correlations and dynamical patterns in these fundamentally multiscale phenomena. We expect that a computational approach to the earthquake problem will produce new models and insights into observations such as GPS and InSAR, much as large-scale computing approaches have had a significant and lasting impact in other areas of science where the underlying phenomena span significant ranges in spatial and temporal scales. Although all scales are important, we place more emphasis on the fault network and system scale, since this is the scale of most observational data networks.

[9] In this paper we will discuss how a statistical physics approach to understanding earthquakes may lead to statistically significant earthquake forecasts. We will first discuss various statistically robust measures of earthquake occurrence. We will then introduce a variety of approaches to material failure that may lead to a better understanding of earthquake occurrence. We will then discuss how the fundamentals of statistical physics can be applied to models that are relevant to the occurrence of earthquakes, and finally we will consider forecasting techniques arising from statistical physics methods that show promise for earthquake forecasting. Research developments over the last decade provide substantial support for the idea that new, systems-level approaches to the numerical simulation of earthquake fault systems, together with new ideas from fundamental approaches to high-dimensional nonlinear systems arising from statistical physics, provide a successful and critically important new path of investigation. An en-

TABLE 1. Earthquake Scaling Regimes[a]

Spatial Scale	*Physics*	*Input From Lower Scale*	*Output to Upper Scale*	*Computational Methods*
Grain size 1 μm to 1 cm	contact interactions, planar fault, elastic walls	cohesive potential across grains	effective viscosity, LG effective constants	MD, PD
Fault zone 1 cm to 100 m	fluidized viscous gouge, elastic walls and interactions, strong correlations	effective viscosity, LG effective constants	effective friction laws, e.g., rate and state, stick-slip, leaky stress, elastic constants, effective LG constants	FD, PD, FEM, CA, BEM, inertial solvers
Fault groups 100 m to 10 km	coarse-grained planar faults, effective friction, strong correlations	effective friction laws, e.g., rate and state, stick-slip, leaky stress, effective elastic constants, effective LG constants	effective elastic moduli, effective friction properties (μ_s, μ_d, β), effective LG constants	CA, BEM, FEM, quasi-static solvers
Fault networks and systems 10–1000 km	complex fault topology, viscoelastic relaxation, static-kinetic friction, strong correlations	effective elastic moduli and friction properties (μ_s, μ_d, β), effective LG constants	effective viscosity spectrum, effective viscoelastic modulus spectrum	CA, BEM, GeoFEM
Tectonic plate boundary	viscoelastic flow on very long timescales, kinematics of plate motion at fault velocity V	effective viscosity spectrum, effective viscoelastic modulus spectrum	no larger scale of interest	GeoFEM

[a]FEM, finite element method; GeoFEM, Japanese Geo FEM software; MC, Monte Carlo; DFT, density functional theory; FD, finite difference; MD, molecular dynamics; PD, particle dynamics; LG, Landau-Ginzburg; CA, cellular automata; and BEM, boundary element method.

hanced program of numerical simulations can be used either in the development of ensemble and other forecasting techniques or as a numerical laboratory in which rigorous hypotheses can be posed, evaluated, and tested [*Rundle et al.*, 2000d, 2001; Solid Earth Research Virtual Observatory Grid, http://www.servogrid.org/, 2002; Asia Pacific Economic Cooperation for Earthquake Simulations, http://quakes.earth.uq.edu.au/ACES/, 2002].

2. EARTHQUAKE SCALING

[10] The Earth's crust is clearly extremely complex, and earthquake statistics exhibit many random aspects. However, despite this complexity, there are several universally valid scaling relations.

2.1. Frequency-Magnitude Statistics

[11] The best known scaling relation for earthquakes is the Gutenberg-Richter frequency-magnitude relation [*Gutenberg and Richter*, 1954]

$$\log N_{GR}(>m) = -b\,m + a \ , \qquad (2)$$

where N_{GR} is the (cumulative) number of earthquakes with a magnitude greater than m occurring in a specified area and time and b and a are constants. This relation is valid for earthquakes both regionally and globally. The constant b or "b value" varies from region to region but is generally in the range of $0.8 < b < 1.2$ [*Frohlich and Davis*, 1993]. The constant a is a measure of the regional level of seismicity. There are a variety of measures for the magnitude, including local, body wave, surface wave, and moment magnitude [*Lay and Wallace*, 1995]. In general, for small earthquakes ($m < 5.5$) these different magnitude measures give approximately equivalent results.

[12] Although the Gutenberg-Richter frequency-magnitude relation was originally developed as an empirical relation, we now recognize that it belongs to a broad range of natural phenomena that exhibit fractal scaling [*Turcotte*, 1989, 1997]. For earthquakes, fractal scaling implies the validity of the relation

$$N_{GR} = C\,A^{-\gamma} \ , \qquad (3)$$

where N_{GR} is the (cumulative) number of earthquakes with rupture areas greater than A occurring in a specified area and time; C and γ are constants with $D = 2\gamma$ the fractal dimension. *Aki* [1981] showed that equations (2) and (3) are entirely equivalent with

$$\gamma = b = \frac{D}{2} . \qquad (4)$$

Thus the universal applicability of the Gutenberg-Richter relation implies universal fractal behavior of earthquakes.

[13] As an example of the validity of Gutenberg-Richter scaling we consider seismicity in southern California.

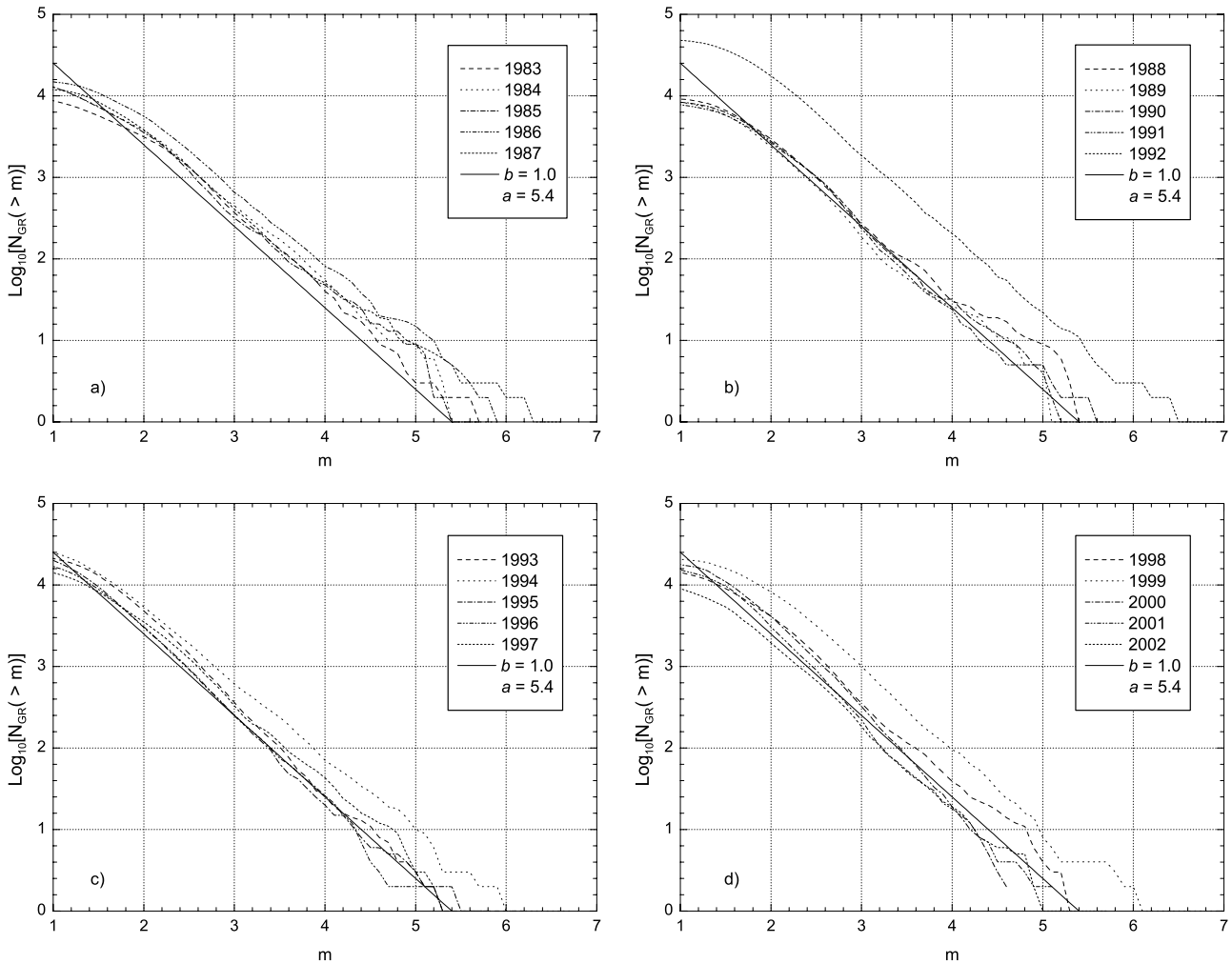

Figure 1. Cumulative number of earthquakes per year, N_{GR}, occurring in southern California with magnitudes greater that m as a function of m. Twenty individual years are considered (SCSN catalog, 2003): (a) 1983–1987, (b) 1988–1992, (c) 1993–1997, and (d) 1998–2002. The solid straight line in Figures 1a–1d is the Gutenberg-Richter relation (2) with $b = 1.0$ and $a = 5.4$. The larger number of earthquakes in 1987, 1992, 1994, and 1999 can be attributed to the aftershocks of the Whittier-Narrows, Landers, Northridge, and Hector Mine earthquakes, respectively. If aftershocks are excluded, the background seismicity in southern California is nearly uniform in time.

The frequency-magnitude distributions of the regional seismicity in southern California on a yearly basis are plotted in Figure 1 using data obtained from the SCSN catalog (2003). For each individual year between 1983 and 2002 the cumulative number of earthquakes N_{GR} with magnitudes greater than m is plotted as a function of m. The period 1983–2003 taken together results in the Gutenberg-Richter power law relation (2) with $b = 1.0$ and $a = 5.4$, shown as the solid straight lines in Figures 1a–1d. In Figure 1, there is generally good agreement between each individual year's data and the Gutenberg-Richter relation (solid straight line) for the period 1983–2003. The exceptions can be attributed to the aftershock sequences of the 1987 Whittier-Narrows, 1992 Landers, 1994 Northridge, and 1999 Hector Mine earthquakes.

[14] With aftershocks removed, the background seismicity in southern California illustrated in Figure 1 is nearly uniform from year to year and is not a function of time. Small earthquakes behave like thermal background noise. There is observational evidence that the Earth's crust is continuously on the brink of failure [*Scholz*, 1991]. One example is induced seismicity. Whenever the crust is loaded, earthquakes are induced whether in a tectonically active area or not. Examples of nontectonic loading include the filling of a reservoir behind a newly completed dam or the high-pressure injection of fluids in a deep well.

2.2. Temporal Decay of Aftershocks

[15] A universal scaling law describes the temporal decay of aftershock activity following an earthquake. This is known as the modified Omori's law and as most widely used has the form [*Scholz*, 2002]

$$\frac{dN_{as}}{dt} = \frac{1}{t_0\,(1 + t/t_1)^p}\ , \tag{5}$$

where N_{as} is the number of aftershocks with magnitudes greater than a specified value, t is time measured forward from the occurrence of the main shock, t_0 and t_1 are constants, and the power p has a value near $p \approx 1$. When an earthquake occurs, there are regions where the stress is increased. This increase in stress is the fundamental cause of aftershocks. However, the systematic time delay before the occurrence of aftershocks requires an explanation. *Das* and *Scholz* [1981] have attributed this delay to stress corrosion combined with a critical stress intensity factor. *Shaw* [1993] has utilized a phenomenological approach to the dynamics of subcritical crack growth. A time delay is implicit in the empirically derived rate and state friction law. *Dietrich* [1994] has related the power law decrease in aftershock activity to this law. Time delays are also associated with the failure of composite materials and other engineering materials. Damage mechanics is a widely used empirical approach to these problems. *Main* [2000] and *Shcherbakov and Turcotte* [2003b] have explained the power law decay of aftershocks in terms of damage mechanics. There appear to be fundamental similarities between aftershock delays and the nucleation of bubbles in a superheated liquid. These similarities led *Rundle* [1989], *Rundle and Klein* [1993], and *Rundle et al.* [1999] to relate aftershock sequences to the power law scaling in the vicinity of a spinodal line. This association is also supported by the relationship between the three-dimensional spatial distributions of aftershocks and the "backbone" of a three-dimensional percolation cluster given by *Robertson et al.* [1995].

[16] Another approach to explain the occurrence of aftershocks is based on a branching stochastic process. The epidemic-type aftershock model has been introduced by *Kagan and Knopoff* [1981, 1987] and *Ogata* [1988] and studied in detail by *Helmstetter and Sornette* [2002a, 2002b] and *Helmstetter et al.* [2003]. In this model each event is capable of producing secondary aftershock sequences and can be considered simultaneously as a foreshock, main shock, or aftershock. The resulting aftershock sequence is a combined effect of many aftershock sequences produced by each aftershock.

2.3. Accelerated Moment Release

[17] There is also accumulating evidence that there may be an increase in the number of intermediate-sized earthquakes prior to a large earthquake. The occurrence of a relatively large number of intermediate-sized earthquakes in northern California prior to the 1906 San Francisco earthquake has been noted by *Sykes and Jaumé* [1990]. These authors also pointed out increases in intermediate-sized events before the 1868 Hayward and 1989 Loma Prieta events in northern California. *Ellsworth et al.* [1981] first pointed out that the rate of intermediate-sized events in the San Francisco Bay region started increasing about 1955 from its post-1906 low. It has also been suggested that there is a power law increase in seismicity prior to a major earthquake as first proposed by *Bufe and Varnes* [1993]. They considered the cumulative amount of Benioff strain in a specified region. The cumulative Benioff strain $\varepsilon_B(t)$ attributed to a precursory earthquake is defined by

$$\varepsilon_B(t) = \sum_{i=1}^{N(t)} \sqrt{e_i}\ , \tag{6}$$

where e_i is the seismic energy release of the ith precursory earthquake and $N(t)$ is the number of precursory earthquakes considered up until the time t. *Bufe and Varnes* [1993] showed that an accurate retrospective prediction of the Loma Prieta earthquake could be made by assuming a power law increase in Benioff strain prior to the earthquake. This power law increase takes the form

$$\varepsilon_B(t) = \varepsilon_0 - B\ (\Delta t)^s\ , \tag{7}$$

where ε_0 is the cumulative Benioff strain at the time of the characteristic earthquake and Δt is nondimensional time remaining until the next characteristic earthquake given by

$$\Delta t = 1 - t/t_f\ , \tag{8}$$

where t is the time measured forward from the previous characteristic earthquake and t_f is the time interval between characteristic earthquakes. Just after a characteristic earthquake we have $\Delta t = 1$; the next characteristic earthquake occurs at $\Delta t = 0$. The constants B and s are used to fit the data.

[18] Systematic increases in intermediate-level seismicity prior to a large earthquake have been proposed by several authors [*Varnes*, 1989; *Bufe et al.*, 1994; *Knopoff et al.*, 1996; *Varnes and Bufe*, 1996; *Brehm and Braile*, 1998, 1999a, 1999b; *Robinson*, 2000]. A systematic study of the optimal spatial region and magnitude range to obtain the power law seismic activation has been carried out by *Bowman et al.* [1998]. Four examples of their results are given in Figure 2, where the cumulative Benioff strain $\varepsilon(t)$ has been correlated (solid line) with equation (7). Clear increases in seismic activity prior to the 1952 Kern County, 1989 Loma Prieta, 1992 Landers, and 1983 Coalinga earthquakes are illustrated.

[19] It has also been argued that the accelerated seismic release exhibits a log-periodic behavior in addition to the power law increase given in equation (7) [*Sornette and Sammis*, 1995; *Saleur et al.*, 1996b; *Sornette*, 1998; *Sammis and Sornette*, 2002]. However, this behavior is not widely accepted.

[20] In obtaining the data given in Figure 2, *Bowman et al.* [1998] investigated circular regions about each of the characteristic earthquakes they considered. They determined the optimal radius for activation. *Sornette and Sammis* [1995] associated this precursory activation

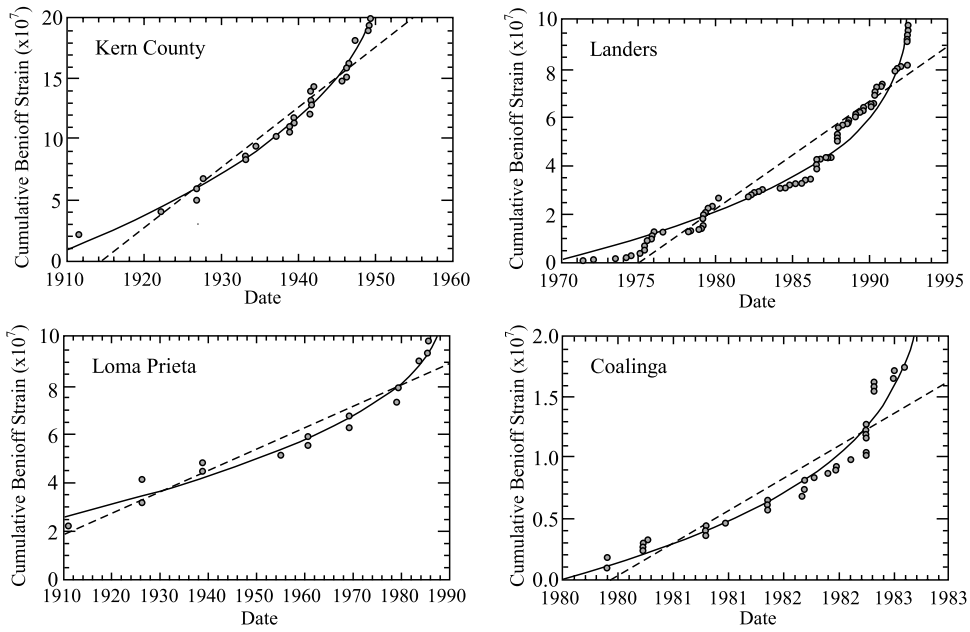

Figure 2. Data points are cumulative Benioff strains $\varepsilon(t)$ determined from equation (6) prior to four major earthquakes in California [*Bowman et al.*, 1998]. Clear increases in seismic activity prior to the 1952 Kern County, 1989 Loma Prieta, 1992 Landers, and 1983 Coalinga earthquakes are illustrated. In each of the four examples the data have been correlated (solid lines) with the power law relation given in equation (7). The values of the power law exponent s used in equation (7) are given in Table 2. Dashed straight lines represent a best fit constant rate of seismicity.

with the approach to a critical phase transition. *Saleur et al.* [1996a, 1996b] interpreted this behavior in terms of correlation lengths that increase prior to the characteristic earthquake. Thus we will refer to this radius of the optimal activation region as an activation correlation length (ACL).

[21] The power law exponents s and the ACL ξ for the 12 earthquakes studied by *Bowman et al.* [1998] are given in Table 2. The mean value of s for these earthquakes is $\bar{s} = 0.26 \pm 0.15$ (error given is 1 standard deviation). Using similar approaches to the accelerated moment release, ACLs of other earthquakes have been obtained by *Brehm and Braile* [1998, 1999a] and by *Robinson* [2000]. All of these data are given in Figure 3. Activation correlation lengths are given as a function of earthquake magnitude and the characteristic rupture length. Although there is considerable scatter, there is a clear increase in the ACL with increasing earthquake magnitude. Also included for comparison is the relation

$$\xi = 10\, A^{1/2}. \tag{9}$$

Many of the ACLs are greater than 10 times the characteristic rupture length.

[22] *Dobrovolsky et al.* [1979] and *Keilis-Borok and Kossobokov* [1990] reported a similar scaling for the maximum distance between an earthquake and its precursors using pattern recognition techniques. Large ACLs are also suggested by the remotely triggered af-

TABLE 2. Observed Earthquake Scales

Earthquake	*Date*	*Magnitude*	ξ, *km*	*s*
Assam	15 August 1950	8.6	900 ± 175	0.22
San Francisco	18 April 1906	7.7	575 ± 240	0.49
Kern County	21 July 1952	7.5	325 ± 75	0.30
Landers	28 June 1992	7.3	150 ± 15	0.18
Loma Prieta	18 October 1989	7.0	200 ± 30	0.28
Coalinga	2 May 1983	6.7	175 ± 10	0.18
Northridge	17 January 1994	6.7	73 ± 17	0.10
San Fernando	9 February 1971	6.6	100 ± 20	0.13
Superstition Hill	24 November 1987	6.6	275 ± 95	0.43
Borrego Mountain	8 April 1968	6.5	240 ± 60	0.55
Palm Springs	8 July 1986	5.6	40 ± 5	0.12
Virgin Islands	14 February 1980	4.8	24 ± 2	0.11

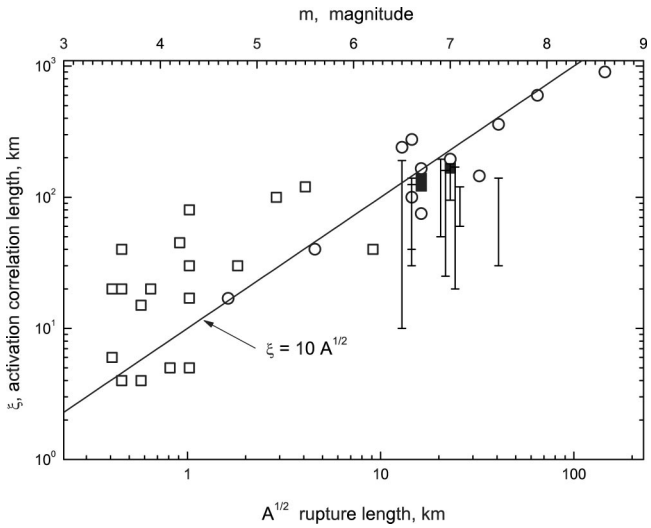

Figure 3. Correlation lengths ξ for precursory seismic activation are given as a function of the square root of the rupture area and the earthquake magnitude m. The circles are the values given by *Bowman et al.* [1998] and tabulated in Table 2. The open squares are values obtained for earthquakes in the New Madrid seismic zone by *Brehm and Braile* [1998]. The error bars are limits obtained for earthquakes in the western United States by *Brehm and Braile* [1999b]. The solid squares are values obtained for earthquakes in New Zealand by *Robinson* [2000].

tershocks following the Landers, California, earthquake [*Hill et al.*, 1993].

[23] The seismic activation hypothesis is illustrated in Figure 4 [*Rundle et al.*, 2000a]. The cumulative frequency-magnitude distribution of earthquakes is shown for three time periods during the earthquake cycle, $1.0 > \Delta t > 0.2$, $0.2 > \Delta t > 0.1$, and $0.1 > \Delta t > 0.0$, where Δt has been defined in equation (8). Small earthquakes occur uniformly at all times but early on in the earthquake cycle $1.0 > \Delta t > 0.2$; there is a systematic lack of intermediate-sized earthquakes. In the time period $0.2 > \Delta t > 0.1$, there is an increase of intermediate-sized events. In the precursory time period $0.1 > \Delta t > 0.0$ this is seismic activation and a further increase in the numbers of intermediate-sized events. Finally, when $\Delta t = 0$, the characteristic earthquake occurs. The first two curves are also evidence of growing correlation lengths as we discuss in section 3. The last curve represents unstable growth of earthquake clusters.

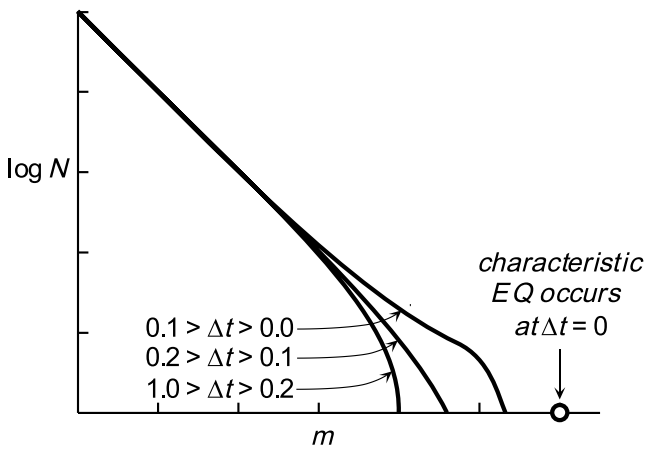

Figure 4. Gutenberg-Richter illustration of the cumulative number of earthquakes occurring per unit time with magnitudes greater than m as a function of m. Data are for different time periods during the earthquake cycle $1 \geq \Delta t \geq 0$ prior to the occurrence of a characteristic earthquake at $\Delta t = 0$. Small earthquakes occur at a constant rate, but there is an activation of intermediate-sized earthquakes prior to the occurrence of the characteristic earthquake.

[24] We further suggest that the behavior described above is nested. The 1992 Landers and 1994 Northridge earthquakes generated precursory activation that will be described in section 3. However, it is likely that the Landers and Northridge earthquakes represent precursory activation that is associated with the next great (characteristic) earthquake on the San Andreas Fault in southern California.

[25] *Zöller et al.* [2001] directly estimated the ACL from earthquake catalogs using single-link cluster analysis [*Frohlich and Davis*, 1990]. They studied 11 earthquakes in California with $m > 6.5$ since 1952 and found systematic increases in the correlation lengths prior to most of these earthquakes. *Main* [1999], *Jaumé and Sykes* [1999], *Jaumé* [2000], *Vere-Jones et al.* [2001], *Bowman and King* [2001], *Zöller and Hainzl* [2001, 2002], and *Ben-Zion and Lyakhovsky* [2002] have provided critical reviews of seismic activation. *Goltz and Bose* [2002] have studied precursory seismic activation using configurational entropy.

[26] An important question that remains unresolved is whether earthquake scaling, as discussed in section 2.1, is associated with the scaling of faults in the crust. It has been shown that the fragmented structure of the crust is fractal over a very wide range of scales [*Sammis et al.*, 1986, 1987; *Sammis and Biegel*, 1989; *Sammis and Stacey*, 1995]. However, an association of this scaling with earthquake scaling has not been demonstrated.

3. PHASE TRANSITION MODEL: NUCLEATION AND CRITICAL PHENOMENA

[27] The observed scaling laws associated with earthquakes have led a variety of researchers [*Rundle*, 1989; *Bowman et al.*, 1998; *Fisher et al.*, 1997; *Mora*, 1999; *Klein et al.*, 2000; *Rundle et al.*, 1996; *Jaumé and Sykes*, 1999; *Turcotte*, 1997] to the conclusion that these events can be regarded as a type of generalized phase transition, similar to the nucleation and critical phenomena that are observed in thermal and magnetic systems [*Ma*, 1976]. The physics of these systems, and their application to earthquake phenomena, has been detailed elsewhere, so we do not repeat these discussions here [*Ma*, 1976; *Gunton and Droz*, 1983]. However, we give a brief summary, as background to the discussions that follow.

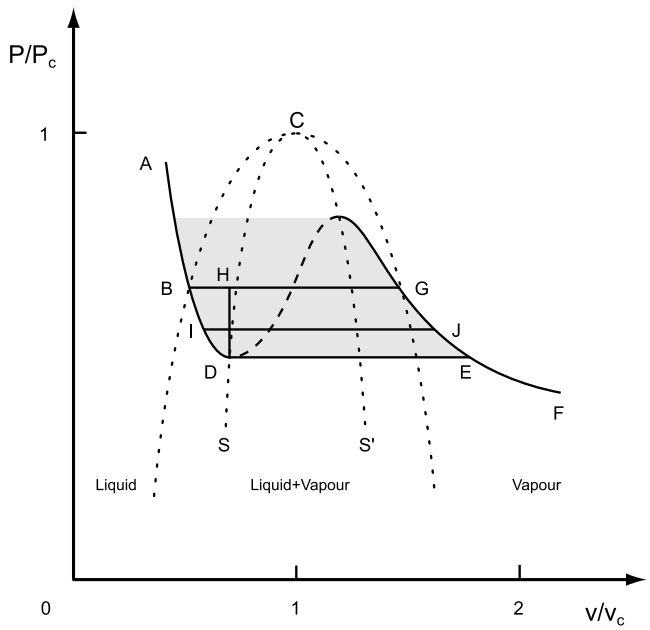

Figure 5. Schematic pressure-volume (P-v) projection of the phase diagram of a pure substance [*Debenedetti*, 1996]. The equilibrium and nonequilibrium behaviors of the liquid-vapor mixture are discussed in the text. The shaded region is metastable.

[28] In order to illustrate the relevant statistical physics we first discuss the phase diagram for the coexistence of the liquid and vapor phases of a pure substance. A schematic pressure-volume projection of a phase diagram is illustrated in Figure 5 [*Debenedetti*, 1996]. We consider a liquid initially at point A in Figure 5. The pressure is decreased isothermally until the coexistence point is reached at point B. In thermodynamic equilibrium the liquid will boil at constant pressure and temperature until it is entirely a vapor at point G. Further reduction of pressure will result in isothermal expansion of the vapor along path GF. However, it is possible to create a metastable, superheated liquid at point B. If bubbles of vapor do not form or are rapidly reabsorbed by the fluid, either by homogenous or heterogeneous nucleation, the liquid can be superheated along path BD. The point D is the intersection of the liquid P–v curve with the spinodal curve S. It is not possible to superheat a liquid beyond this point. If the liquid is superheated to the vicinity of point D, explosive nucleation and boiling (instability) will take place. If the pressure and temperature are maintained constant during this highly nonequilibrium explosion, the substance will follow path DE to the vapor equilibrium curve GF. If the explosion occurs at constant volume and temperature, the pressure will increase as the substance follows the path DH to the equilibrium boiling line BG. Any horizontal path between the superheated liquid BD and vapor GE is possible. An example is the path IJ. The entire shaded region is metastable. The critical point C is at the critical pressure P_c and critical specific volume v_c. A point on a horizontal line, for example IJ, is determined by the "wetness" of the liquid-vapor mixture, the mass fraction that is liquid. At point I the mass fraction of liquid is essentially 1; at point J the mass fraction of liquid is essentially 0. Which path is followed in the metastable region is determined by the physics of the bubble nucleation process [*Debenedetti*, 1996].

[29] At the critical point [*Stanley*, 1971; *Ma*, 1976] the parameters in the equation of state of a substance such as the water liquid-vapor system, which is governed by a Van der Waals–type equation of state, can be shown to specify a location in state space at which the specific heat $c(T)$ has a cusp, or singularity, when plotted as a function of temperature T. Phase transitions of this type are called second-order, since the quantity displaying the singularity $c(T)$ is the second derivative of the thermodynamic free energy. For temperatures T at, or higher than, the critical temperature, the density ρ is a continuous function of pressure P. Laboratory observations demonstrate the existence of very large spatial and temporal fluctuations in the density of the liquid-vapor mixture near the critical point. Observations indicate that these fluctuations are correlated over distance and timescales that are characterized by the correlation length ξ and the correlation time τ, respectively. As the critical point is approached, usually by controlling T and v in some kind of piston-cylinder apparatus, laboratory observations indicate that both ξ and τ diverge ($\xi \rightarrow \infty$ and $\tau \rightarrow \infty$). The divergence of the correlation timescale τ is called critical slowing down. In addition, experiments indicate that $\tau \propto \xi^z$, where z is a dynamic scaling exponent. For diffusive systems a typical value of z is $z = 2$.

[30] Magnetic systems exhibit a similar type of physics at the Curie point, defining the transition from low-temperature ferromagnetic behavior to high-temperature paramagnetic behavior. In these magnetic systems the critical temperature is the Curie temperature T_c, the magnetization M plays a role similar to the density ρ in a liquid-gas system ($M \Leftrightarrow \rho$), and an applied external magnetic field h plays a role similar to the pressure P in liquid-gas systems ($h \Leftrightarrow P$). It is also found that at the Curie point, large fluctuations in M are associated with the transition from ferromagnetism to paramagnetism and that these fluctuations are characterized by diverging length and timescales, ξ and τ, respectively. A common terminology has evolved to describe all such systems. Thus, for example, M and ρ are called the order parameters of the respective systems. These are the physical fields that respond to changes in the control parameters (T, h) or (T, P).

[31] Away from the critical point, phase transitions are first order and are associated with nucleation [*Stanley*, 1971; *Klein and Unger*, 1983; *Klein and Leyvraz*, 1986; *Debenedetti*, 1996; *Klein et al.*, 2000]. In the water liquid-vapor system, nucleation is the process in which bubbles of water vapor form within liquid water prior to boiling. Changes in T or P can make a thermal system unstable to a change in ρ, leading to the appearance of a new

phase. An example is the change of water from a liquid phase to a gas phase as T is increased at constant P. In making the transition from the liquid to the gas phase, the mass of liquid water may progress from its stable equilibrium regime through a region of metastable equilibrium, but it cannot remain as a stable metastable liquid past the classical limit of stability or spinodal line [*Debenedetti*, 1996; *Klein and Unger*, 1983; *Ray and Klein*, 1990; *Rundle et al.*, 2000a]. The existence of a spinodal line is a consequence of the Van der Waals–type equation of state. The spinodal line has a number of interesting properties, the most important of which is that it behaves like a line of critical points for the nucleating droplets of vapor. Near the spinodal line, one observes divergent length scales ξ and timescales τ, as well as the appearance of large fluctuations in ρ and scaling as in the relationship $\tau \propto \xi^z$.

[32] Many real thermal systems can never approach the spinodal line because of the existence of random thermal fluctuations arising from environmental factors. These random fluctuations cause the liquid-vapor transition to occur at very shallow quench depths ("cloud points") in the metastable regime, far from the spinodal line [*Gunton et al.*, 1973]. However, for systems having long-range interactions, such as spin dipoles or elastic forces, these random fluctuations tend to be suppressed at wavelengths less than the range of the interactions because of the spatial averaging effects of the interactions. Thus each molecule or spin sees only the average field, or mean field, of all the other interacting molecules or spins [*Klein and Unger*, 1983]. In mean field systems, only the longest wavelength fluctuations survive the averaging effects, leading to a stabilization of the system through the metastable regime. The result is that the metastable phase in mean field systems can approach very near the spinodal line, and so the scaling and other critical phenomena-like properties of the spinodal line can be observed [*Klein et al.*, 2000].

[33] In a system that is near but not at the mean field limit because of long but finite range interactions, the relative size of fluctuations in the order parameter will increase. These fluctuations, which grow increasingly large as the limit of stability (spinodal line) is approached, are due to increasingly large regions of the system condensing into droplets of the "other phase," then evaporating and reverting to the "original phase." One of the large droplets of the "other phase" finally becomes large enough to nucleate the system, and the phase transition then occurs. The same increase in fluctuation amplitude can be observed as the critical point is approached.

[34] The size of the fluctuations in a liquid-gas system is typically measured by the Ginzburg criterion Γ:

$$\Gamma \equiv \frac{\mathrm{Var}\{\rho - \rho_{gas}\}}{|\langle \rho - \rho_{gas} \rangle|^2} \quad . \tag{10}$$

Here $\mathrm{Var}\{\rho - \rho_{gas}\}$ represents the variance of the order parameter, which is the density $\rho - \rho_{gas}$ in a liquid-gas system, and $\langle \rho - \rho_{gas} \rangle$ is the mean. Since the Ginzburg criterion is applied to systems that are in either equilibrium or long-lived metastable equilibrium, all averages are taken over both space and time. In a spin system the fluctuating order parameter is the spin density, and a similar Ginzburg criterion can be written. Typically, the "critical region," indicating proximity of the system to a critical point, is defined by the condition [*Ma*, 1976]

$$\Gamma \geq 10\% \, , \tag{11}$$

which is an indication of large fluctuations. For systems undergoing a first-order phase transition, one expects to see a large value of Γ prior to the occurrence of the transition.

4. BRITTLE FRACTURE

[35] Before addressing the earthquake problem, we will briefly consider the association between brittle failure and statistical physics. The brittle failure of a solid is a complex phenomenon that has received a great deal of attention from engineers, geophysicists, and physicists. A limiting example of brittle failure is the propagation of a single fracture through a homogeneous solid. However, this is an idealized case that requires a preexisting crack or notch to concentrate the applied stress. Even the propagation of a single fracture is poorly understood because of the singularities at the crack tip [*Kanninen and Popelar*, 1985; *Freund*, 1990]. In most cases the fracture of a homogeneous brittle solid involves the generation of microcracks. Initially, these microcracks are randomly distributed; as their density increases, they coalesce and localize until a throughgoing rupture results. This process depends upon the heterogeneity of the solid. There is an analogy between the microcracks leading to fracture and bubble nucleation leading to boiling.

[36] Many experiments on the fracture of brittle solids have been carried out. In terms of rock failure the early experiments by *Mogi* [1962] were pioneering. Acoustic emissions associated with microcracks were monitored, and power law frequency-magnitude Gutenberg-Richter statistics were observed for the acoustic emissions. When a load was applied very rapidly, the time to failure was found to depend on the load. Many other studies of this type have been carried out. *Otani et al.* [1991] obtained the statistical distribution of the lifetimes with constant stress loading for carbon fiber epoxy microcomposites. *Johansen and Sornette* [2000] studied the rupture of spherical tanks of kevlar wrapped around thin metallic liners and found a power law increase of acoustic emissions prior to rupture. *Guarino et al.* [1998, 1999] studied the failure of circular panels (222 mm diameter and 3–5 mm thickness) of chipboard and fiberglass. A differential pressure was either applied rapidly across a

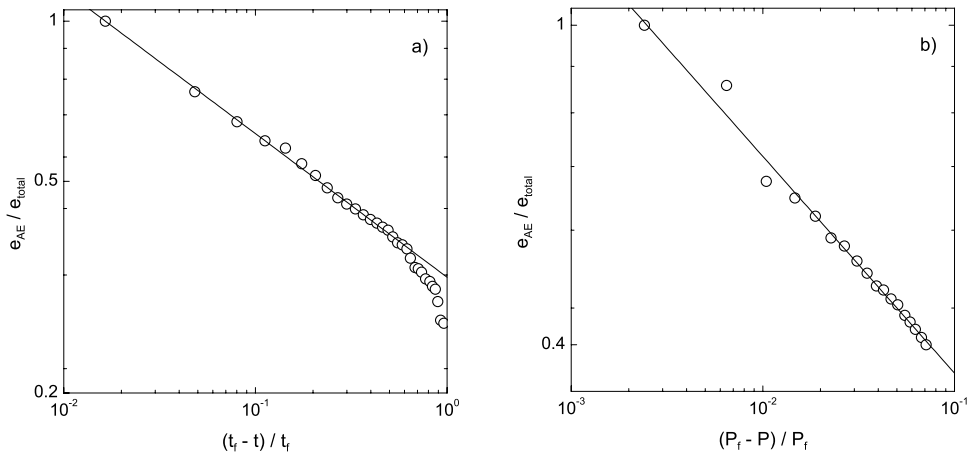

Figure 6. (a) Cumulative acoustic energy emissions $e_{AE}(t)$ at time t divided by the total acoustic energy emissions e_{tot} at the time of rupture ($t = t_f$) as a function of $(1 - t/t_f)$. A constant pressure difference was applied at $t = 0$. The straight line correlation is with $e_{AE} \propto (1 - t/t_f)^{-0.27}$ [*Guarino et al.*, 1999]. (b) Cumulative acoustic energy emissions $e_{AE}(t)$ divided by the total acoustic energy emissions e_{tot} at the time of rupture ($t = t_f$) as a function of $(P_f - P)/P_f$, where P is the applied pressure difference across the failing panel of chipboard and P_f is the pressure difference when the board fails. The applied pressure difference across the panel was increased linearly with time. The straight line correlation is with $e_{AE} \propto (1 - P/P_f)^{-0.27}$ [*Guarino et al.*, 1998].

panel and was held constant until the panel failed or was increased linearly in time until the panel failed. Acoustic emission events associated with microcracks were carefully monitored, located, and quantified. Initially, the microcracks appeared to be randomly distributed across the panel; as the number of microcracks increased, they tended to localize and coalesce in the region where the final rupture occurred. *Guarino et al.* [1998, 1999] also showed that the frequency-magnitude statistics of the acoustic emissions satisfy the power law (Gutenberg-Richter) relation, equations (2) and (3). They also measured the cumulative energy in the acoustic emission events e_{AE} as a function of time t. The total acoustic emission energy at the time of rupture is e_{tot}. The observed dependence of e_{AE}/e_{tot} on $(1-t/t_f)$ for these experiments is given in Figure 6. After an initial transient period, good power law scaling was observed. In this scaling region it was found that $e_{AE} \propto (1-t/t_f)^{-0.27}$. This activation is very similar to the power law seismic activation given in equation (7) illustrated in Figure 2. In the case of a rapid application of pressure, *Guarino et al.* [1999] found a systematic dependence of the time to failure t_f on the applied pressure P. *Shcherbakov and Turcotte* [2003a] correlated this dependence with the relation

$$t_f \propto (P - P_y)^{-2.25} \ , \tag{12}$$

where P_y is a threshold or yield stress.

[37] Statistical physicists have related brittle rupture to liquid-vapor phase changes in a variety of ways. *Buchel and Sethna* [1997] have associated brittle rupture with a first-order phase transition. Similar arguments have been given by *Zapperi et al.* [1997] and *Kun and Herrmann* [1999]. On the other hand, *Sornette and Andersen* [1998] and *Gluzman and Sornette* [2001] argue that brittle rupture is analogous to a critical point phenomena rather than the metastability of a first-order phase change. They associated observed power law scaling in brittle failure experiments with a critical point (a second-order phase change). A number of authors have considered brittle rupture in analogy to nucleation near spinodal line [*Rundle* and *Klein*, 1989; *Selinger et al.*, 1991; *Rundle et al.*, 1997b, 1999, 2000a; *Zapperi et al.*, 1999].

[38] We next apply the concept of phase change to the brittle fracture of a solid. For simplicity, we will discuss the failure of a sample of area a under compression by a force F. The state of the sample is specified by the stress $\sigma = F/a$ and its strain $\epsilon = (L_0 - L)/L_0$ (where L is length and L_0 is initial length). At low stresses we assume that Hooke's law is applicable so that

$$\sigma = E_0 \epsilon \ , \tag{13}$$

where E_0 is Young's modulus, a constant.

[39] We hypothesize that a brittle solid will obey linear elasticity for stresses in the range $0 \le \sigma \le \sigma_y$, where σ_y is a yield stress. From equation (13) the corresponding yield strain ϵ_y is given by

$$\epsilon_y = \frac{\sigma_y}{E_0} \ . \tag{14}$$

If stress is applied infinitely slowly (to maintain athermodynamic equilibrium), we further hypothesize that the solid will fail at the yield stress σ_y. The failure path ABG in Figure 7 corresponds to the equilibrium failure path ABG in Figure 5. This is equivalent to perfectly plastic behavior. We draw an analogy between the phase

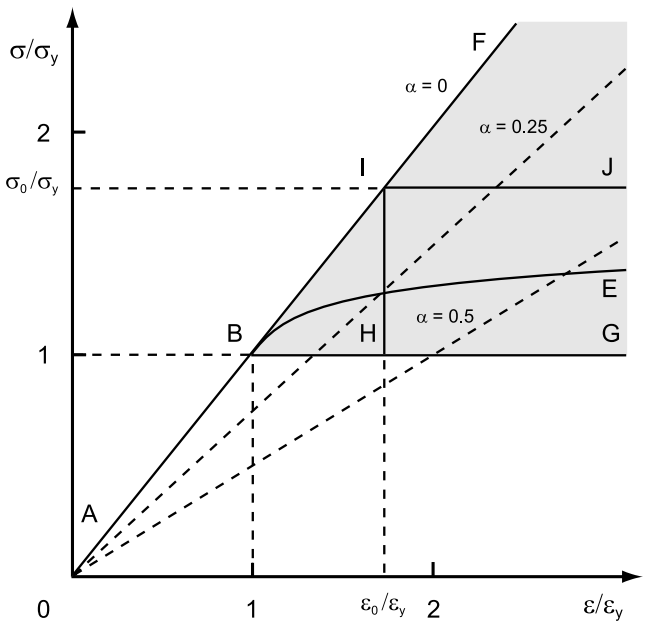

Figure 7. Idealized stress-strain diagram for a brittle solid. It is hypothesized that the solid behaves as a linear elastic material at stresses less that the yield stress σ_y and strains less than the yield strain ϵ_y (path AB). Failure at an intermediate constant rate of stress increase takes place along path ABE. The dashed lines correspond to constant values of the damage variable α.

change behavior illustrated in Figure 5 and the inelastic deformation of a solid illustrated in Figure 7. Pressure P is analogous to stress σ, and specific volume v is analogous to strain ϵ.

[40] If an elastic solid is loaded very rapidly with a constant stress $\sigma_0 \leq \sigma_y$ applied instantaneously, the solid will satisfy equation (13) and will follow the path ABI as shown in Figure 7. Subsequently, damage will occur at a constant stress along the path IJ until the solid fails. This behavior is analogous to the constant pressure boiling that occurs along path DE in Figure 5.

[41] Alternatively, the elastic solid could be strained very rapidly with a constant strain $\epsilon_0 \leq \epsilon_y$ applied instantaneously, and again the solid will satisfy equation (13) and follow the path ABI as shown in Figure 7. In this case, damage will occur along the constant strain path IH until the stress is reduced to the yield stress σ_y. This behavior is analogous to the constant volume boiling that occurs along the path DH in Figure 5.

[42] *Shcherbakov and Turcotte* [2003b] have argued that this stress relaxation process is applicable to the understanding of the aftershock sequence that follows an earthquake. During an earthquake some regions in the vicinity of the earthquake experience a rapid increase of stress (strain). The stress σ is greater than the yield stress σ_y, and microcracks (aftershocks) relax the stress to σ_y just as illustrated in Figure 7. The time delay of the aftershocks relative to the main shock directly corresponds to the time delay of the damage. The delay results because it takes time to nucleate microcracks (aftershocks).

[43] When the stress on a brittle solid is increased at a constant finite rate, linear elasticity (equation (13)) is applicable in the range $0 \leq \sigma \leq \sigma_y$. At stresses greater that the yield stress, $\sigma > \sigma_y$, damage occurs in the form of microcracks. This damage is accelerated strain and a deviation from linear elasticity. A typical failure path ABE is illustrated in Figure 7. In order to quantify the deviation from linear elasticity the damage variable α is introduced in the stress-strain relation

$$\sigma = E_0 (1 - \alpha) \epsilon \ . \tag{15}$$

When $\alpha = 0$, equation (15) reduces to equation (13), and linear elasticity is applicable; as $\alpha \rightarrow 1$ ($\epsilon \rightarrow \infty$), failure occurs. Positions in the stress-strain plot (Figure 7) corresponding to $\alpha = 0.0$, 0.25, and 0.5 are shown. It must be emphasized that the analogy between boiling and fracture illustrated in Figures 5 and 7 is not complete. Boiling is a reversible process; fracture is not. However, we believe the analogy is illustrative.

[44] On the basis of thermodynamic considerations [*Kachanov*, 1986; *Krajcinovic*, 1996; *Lyakhovsky et al.*, 1997] the time evolution of the damage variable is related to the time-dependent stress $\sigma(t)$ and the strain $\epsilon(t)$ by

$$\frac{d\alpha(t)}{dt} = H[\sigma(t)] \left[\frac{\epsilon(t)}{\epsilon_y} \right]^2 \ , \tag{16}$$

where $H[\sigma(t)]$ is known as the hazard rate. It should be noted that there are alternative formulations of both equations (15) and (16) and that $H[\sigma(t)]$ can take many forms [*Krajcinovic*, 1996]. In our analysis we will assume that equations (15) and (16) are applicable and will further require that [*Shcherbakov and Turcotte*, 2003a]

$$H[\sigma(t)] = 0 \ , \qquad 0 \leq \sigma \leq \sigma_y \tag{17}$$

$$H[\sigma(t)] = \frac{1}{t_d} \left[\frac{\sigma(t)}{\sigma_y} - 1 \right]^{\rho} , \qquad \sigma > \sigma_y \ , \tag{18}$$

where t_d is a characteristic timescale for damage and ρ is a power to be determined from experiments. The rate at which damage accumulates is proportional to a power of the stress excess over a yield stress σ_y.

[45] The monotonic increase in the damage variable α given by equations (16)–(18) represents the weakening of the brittle solid due to the nucleation and coalescence of microcracks. This nucleation and coalescence of microcracks is analogous to the nucleation and coalescence of bubbles in a superheated liquid as discussed in section 3. A brittle solid in the shaded region in the stress-strain diagram given in Figure 7 is metastable in the same sense that the nonequilibrium boiling in the shaded region in Figure 5 is metastable.

[46] Solutions of equations (16)–(18) give both the power law activation prior to an earthquake [*Lyakhovsky et al.*, 1997; *Ben-Zion and Lyakhovsky*, 2002; *Turcotte et*

al., 2003] and the power law decay of aftershock activity associated with the modified Omori's law [*Shcherbakov and Turcotte*, 2003b]. *Main* [2000] introduced an empirical strain scaling law for damage and also was able to reproduce power law precursory seismic activation and the power law decay of aftershock activity.

[47] Some forms of damage are clearly thermally activated. The deformation of solids by diffusion and dislocation creep is an example. The ability of vacancies and dislocations to move through a crystal is governed by an exponential dependence on absolute temperature with a well-defined activation energy. The role of temperature in brittle fracture is unclear. *Guarino et al.* [1998] varied the temperature somewhat in their experiments on the fracture of chipboard and found no effect. A systematic temperature dependence of rate and state friction was documented by *Nakatani* [2001]. This has also been shown to be true for the lifetime statistics of kevlar fibers [*Wu et al.*, 1988].

[48] Time delays associated with bubble nucleation in a superheated liquid are explained in terms of thermal fluctuations. The fluctuations must become large enough to overcome the stability associated with surface tension in a bubble. The fundamental question in damage mechanics is the cause of the delay in the occurrence of damage. This problem has been considered in some detail by *Ciliberto et al.* [2001]. These authors attributed damage to the "thermal" activation of microcracks. An effective "temperature" can be defined in terms of the amplitude of random elastic vibrations of the solid. The spatial variability of stress in the solid is caused by the microcracking itself not by thermal fluctuations. This microcracking occurs on a wide range of scales.

5. DISCRETE MODELS

5.1. Fiber Bundle Model

[49] Another approach to the brittle failure is applicable to composite materials. A composite material is made up of strong fibers embedded in a relatively weak matrix. Failures of composite materials have been treated by many authors using the concept of fiber bundles [*Smith and Phoenix*, 1981; *Curtin*, 1991; *Newman and Phoenix*, 2001]. The failure statistics of the individual fibers that make up the fiber bundle are specified. The statistics can be either static or dynamic. In the static case the probability of the failure of a fiber is specified in terms of the stress on the fiber. Failure is assumed to occur instantaneously. In the dynamic case the statistical distribution of times to failure for the fibers is specified in terms of stresses on the fibers [*Coleman*, 1956, 1958]. Experiments generally favor the dynamic failure, fiber bundle models. When stress is applied to a fiber bundle, the fibers begin to fail. It is necessary to specify how the stress on a failed fiber is redistributed to the remaining sound fibers [*Smith and Phoenix*, 1981]. In the uniform load sharing hypothesis the stress from a failed fiber is redistributed equally to the remaining fibers. This is a mean field approximation. The alternative redistribution model is the local load sharing hypothesis. In this case the load on the failed fiber is redistributed to neighboring fibers. Local load sharing is applicable to strongly bonded fibrous (composite) materials, whereas equal load sharing is applicable to weakly bonded fibrous materials.

[50] *Krajcinovic* [1996] and *Turcotte et al.* [2003] have shown that the mean field fiber bundle model with dynamic failure statistics gives a solution for the failure of the bundle that is identical to that obtained using the damage equations (16)–(18). The continuum damage equation and the discrete fiber bundle model give identical results for the transient failure of a brittle material. The coupled failure of fibers is directly analogous to the coupled microcracks associated with damage.

5.2. Sandpile Model

[51] The concept of self-organized criticality [*Turcotte*, 1997, 1999; *Jensen*, 1998] evolved from the "sandpile" model proposed by *Bak et al.* [1988]. In this model, there is a square grid of boxes, and at each time step a particle is dropped into a randomly selected box. When a box accumulates four particles, they are redistributed to the four adjacent boxes, or in the case of edge boxes they are lost from the grid. Since only nearest-neighbor boxes are involved in the redistribution, this is a cellular automata model. Redistributions can lead to further instabilities and avalanches of particles in which many particles may be lost from the edges of the grid. The input is the steady state addition of particles. A measure of the state of the system is the average number of particles in the boxes. This "density" fluctuates about a quasi-equilibrium value. Each of the multiple redistributions during a time step contributes to the size of the model avalanche. One measure of the size of a model avalanche is given by the number of particles lost from the grid during multiple redistributions; an alternative measure of size is the number of boxes that participate in multiple redistributions. According to *Bak et al.* [1988] a system is in a state of self-organized criticality if it is maintained near a critical point. The system is in a marginally stable state when perturbed from this state, it will evolve naturally back to the state of marginal stability. In the critical state, there is no longer a natural length scale so that fractal statistics are applicable. However, this definition is controversial as we will show when considering the related forest fire and slider block models.

5.3. Forest Fire Model

[52] The forest fire model [*Bak et al.*, 1992; *Drossel and Schwabl*, 1992] has many similarities to the sandpile model but also has important differences. The standard forest fire model consists of a square grid of sites. At each time step a model tree is dropped on a randomly chosen site; if the site is unoccupied, the tree is planted. The sparking frequency f_s is the inverse number of

attempted tree drops on the square grid before the model match is dropped on a randomly chosen site. If $f_s = 1/100$, there have been 99 attempts to plant trees (somesuccessful and some unsuccessful) before a match is dropped at the 100th time step. If the match is dropped on an empty site, nothing happens. If it is dropped on a tree, the tree ignites, and a model fire consumes that tree and all adjacent (nondiagonal) trees.

[53] Having specified the size of the square grid and the sparking frequency f_s, a simulation is run for N_s time steps, and the number of fires N_F with area A_F is determined. The area A_F is the number of trees that burn in a fire. In all cases the number of small fires N_F scales with their area A_F in good agreement with the fractal relation (3). If f_s is relatively large, the power law region is confined to small fires. If f_s is small, fires occur that span the grid, and there is a peak in the frequency-magnitude distribution for large fires. The parameter f_s can be "tuned" so that fires cross the grid, but it is not clear that this is a critical point. In terms of self-organized criticality the steady input is the planting of trees, the "avalanches" are the fires, and the number of trees on the grid fluctuates about the quasi-equilibrium value.

[54] The forest fire model is also characterized by a frequency-size distribution of clusters, which is directly related to the frequency-size distribution of fires; both are fractal. Studies of the forest fire model show that clusters of trees continuously grow in size. Small fires sample the frequency-size distribution of clusters, but only a small fraction of the small clusters are lost in the fires. Significant numbers of trees are lost only in the largest fires. *Malamud et al.* [1998] have shown that actual forest fires also exhibit near-fractal frequency-area scaling.

[55] A simple multiplicative-cascade model has been introduced to explain the behavior of the forest fire model and to provide insights into self-organized criticality [*Turcotte*, 1999; *Gabrielov et al.*, 1999]. Clusters of trees grow as trees are planted. Large clusters are created primarily by the coalescence of smaller clusters. Clusters are also lost, but the loss rate is proportional to the number of clusters, whereas the rate at which clusters combine is proportional to the number of clusters squared. Thus significant losses occur only for the very largest clusters. The combination of clusters leads to a scaling region with a fractal frequency-size distribution. This scaling is terminated when a significant number of clusters are lost in fires.

[56] An important question is the relationship of self-organized criticality to ordinary critical phenomena. The site percolation model is a classic critical point problem that is closely related to the forest fire model. Again, a square grid of points is considered, and trees are planted on a site with a probability p. This probability can be "tuned" until a cluster of trees spans the grid; this is the critical point. Clusters do not combine, and trees are not lost in fires. The frequency-size distribution is fractal only in the immediate vicinity of the critical point.

5.4. Slider Block Models

[57] The family of high-dimensional dynamical models with the most direct relevance to simulating the behavior of earthquake faults is slider block models. The first slider block model with massive blocks was the model of *Burridge and Knopoff* [1967]. The first cellular automaton slider block model having massless blocks was given by *Rundle and Jackson* [1977]. The first mean field slider block model was discussed by *Rundle and Klein* [1993].

[58] Consider a single block of mass m pulled over a surface by constant velocity V driver plate. The driver plate is attached to the slider block by a loader spring with spring constant k_L. The interaction of the block with the surface is controlled by friction in some form. The static frictional threshold, associated with the static coefficient of friction, determines the force required to initiate slip of the block. A variety of laws have been proposed for the dynamic friction operative during slip. According to the classical Coulomb-Mohr friction law, stick-slip behavior is observed if the kinetic (dynamic) friction is less than the static friction. The dynamic friction can be taken to be constant, a function of the slip velocity or, more generally, a function of both slip velocity and slip history (rate and state friction). For a single slider block the stick-slip behavior results in periodic slip events. This behavior is analogous to the classical hypothesis of periodic characteristic earthquakes on major faults [*Schwartz and Coppersmith*, 1984].

[59] Now consider the behavior of a pair of slider blocks rather than just a single block as above. Both blocks are attached to a constant velocity driver plate by loader springs, each having spring constant k_L. The blocks are connected to each other with a connecting spring, where the connecting spring constant k_C is not necessarily equal to the loader spring constant k_L. The ratio of the spring constants $\beta = k_L/k_C$ determines the stiffness of the system. If $\beta \gg 1$, the stiff system tends to behave as a single block with periodic slip events. If $\beta = 0$, each of the blocks has periodic, independent slip events. In between these two limits a wide range of interesting behaviors can occur. If the system is symmetric (equal masses, friction, and connecting spring constants), periodic behavior is also observed. However, if the symmetry is broken (i.e., nonequal masses), the pair of slider blocks exhibits deterministic chaos [*Huang and Turcotte*, 1990]. The period-doubling route to chaos is observed with positive values of the Lyapunov exponent in the chaotic regions. The pair of slider blocks is a fourth-order dynamical system (the velocity and displacement of each block), and the behavior is very similar to that of the Lorenz equations [*Lorenz*, 1963] and the logistic map [*May*, 1976]. The behavior is quasiperiodic and cannot be predicted with certainty.

[60] The chaotic behavior of the low-dimensional Lorenz equations (third order) is now accepted as evidence that the behavior of the atmosphere and oceans is chaotic [*Palmer*, 1991; *Read*, 1993]. Similarly, the chaotic

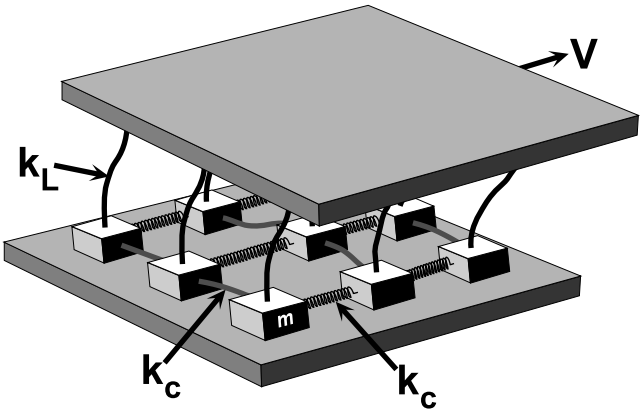

Figure 8. Illustration of the two-dimensional slider block model. An array of blocks, each with mass m, is pulled across a surface by a driver plate at a constant velocity V. Each block is coupled to the adjacent blocks with either leaf or coil springs (spring constant k_C) and to the driver plate with leaf springs (spring constant k_L).

behavior of a pair of slider blocks is evidence that earthquakes might exhibit chaotic behavior. Chaotic behavior has led to the concept of ensemble weather forecasting. The sensitivity of a forecast to initial conditions is taken to be a measure of the reliability of a forecast. Similarly for earthquakes, absolute prediction of the time and place of an event is not possible for a chaotic system. However, probabilistic forecasts are certainly possible, and it may also be possible to utilize ensemble techniques to establish the reliability of forecasts.

[61] Since the pioneering work of *Burridge and Knopoff* [1967] many studies of multiple slider block models have been carried out. The standard multiple slider block model consists of a square array of slider blocks as illustrated in Figure 8. In its simplest form the blocks have equal masses, are connected to the constant velocity driver plate with loader springs (spring constant k_L), and are connected to each other with connecting or coupling springs (spring constant k_C). If the Coulomb-Mohr static-dynamic friction law is assumed to hold, the static coefficient of friction μ_s and the kinetic (dynamic) coefficient of friction μ_d must be specified. It is further assumed that motion of the driver plate is so slow that it is appropriate to neglect its motion during a slip event. The behavior of this model is then controlled by the size of the $n \times n$ array, the stiffness of the system $\beta = k_L/k_C$, and the ratio of static to kinetic friction.

[62] Many other variations on these models have been considered in the literature, and comprehensive reviews have been given by *Carlson et al.* [1994], *Rundle and Klein* [1995a], and *Turcotte* [1997, 1999]. Variations include the following:

5.4.1. Method of Solution

[63] We discuss two solutions: (1) Molecular dynamics (MD) solutions allow many blocks to slip simultaneously during a multiple-block slip event. The required numerical codes are very similar to the MD codes used to study the behavior of solids, which simply solve Newton's second law equations for particles moving in the combined potential of all the other particles. (2) Cellular automata (CA) solutions are those in which the first block that becomes unstable is allowed to complete its motion before a second block is allowed to slip. This approach greatly simplifies computations since only one equation must be solved at a time.

[64] Another way of stating the difference between these two solution methods is that one solves differential equations deterministically in the MD case in two space dimensions plus one time dimension, whereas the CA models typically use a Monte Carlo update scheme with the model defined on a spatial lattice of two dimensions. In the CA case, time is defined in units of Monte Carlo sweeps that can be related to actual time via the various dimensional constants in the problem [*Binder and Heermann*, 1997]. CA simulations often have considerable physical meaning since most interesting nonlinear processes have a strong stochastic component, and the resulting probability distributions are the relationships to be compared to data. CA simulations also have the distinct advantage of being far faster to run on modern computers, so very large systems sizes can be used, and finite size effects are consequently minimized. By contrast, MD simulations are extremely computing intensive, so simulations are frequently limited to small system sizes (a few hundred particles) and very short time intervals (typically microseconds or less for the entire run). Deterministic simulations are also often less "rigorous" than they appear, since the values for the many parameters entering the models are usually not well known or not known at all.

[65] It should be noted that care must be taken in interpreting solutions. *Morein et al.* [1997] considered the motion of slider blocks with static friction but zero dynamic friction. No driver plate was used, and energy was conserved. Using a mean field CA approach with long-range spring, thermolization of the initial energy was found. However, *Morein and Turcotte* [1998] considered the same problem using the MD approach, with no noise and with nearest-neighbor springs and found normal mode solutions which behaved as solitons.

5.4.2. Inertia

[66] If the CA approach is used, the inertia (mass) of a block is neglected. The final state of a block after slip is then specified by a jump or transition rule. Otherwise, if masses are not neglected, the differential equations of motion (Newton's second law) must be solved. In the CA approach, only a single equation requires solution, whereas in the MD approach with nearest-neighbor springs the simultaneous solution of many equations is required.

5.4.3. Range of Interaction

[67] The range of interaction specifies how many adjacent blocks to which each block is coupled via a spring or alternative mechanism for stress transmission, such as bulk elasticity. There are a variety of possibilities: (1) nearest-neighbor redistribution, in which stress is transferred to or from only the nearest-neighbor blocks as illustrated in Figure 8; (2) equal redistribution, in which the stress transfer is equally redistributed to all other blocks, representing a "flat interaction" approximation; and (3) long-range interactions, which can be either of the flat interaction approximation (strength of interaction independent of the distance) or perhaps via an inverse power of distance. Stress is redistributed to q other blocks as a function of the block's distance from the slipping block. In the extreme case of redistribution from one block to all other blocks, fluctuations in stress (force) are averaged out, and one approaches the mean field regime, where each block is considered to interact with the mean field produced by all other blocks. For example, it can be shown that if each block interacts with q other blocks by means of a flat interaction, with each block-block interaction having strength k_C, then the mean field condition is increasingly approached as $qk_C \rightarrow \infty$ [*Klein et al.*, 2000]

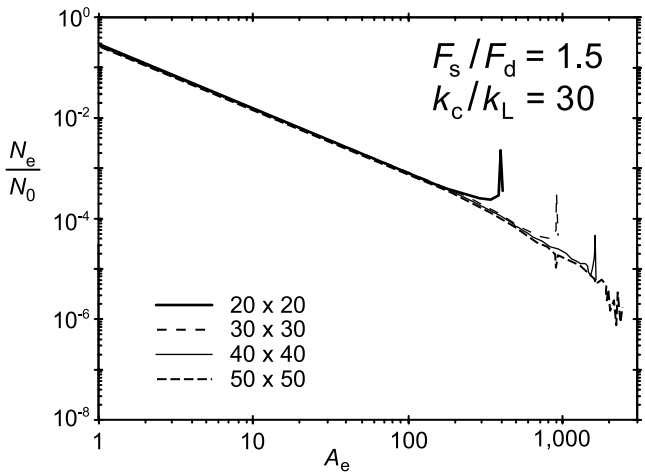

Figure 9. Results of simulations for a two-dimensional slider block model with multiple blocks [*Huang et al.*, 1992]. The ratio of the number of slip events N_e, with area A_e, to the total number of slip events N_0 is plotted against A_e, the number of blocks involved in an event [*Huang et al.*, 1992]. Results are given for systems with stiffness $k_C/k_L = 30$, friction $F_s/F_d = 1.5$, and grid sizes 20×20, 30×30, 40×40, and 50×50. The peaks at $A_e = 400$, 900, and 1600 correspond to catastrophic slip events involving the entire system. From *Huang et al.* [1992], reprinted with permission of Blackwell Publishing.

5.4.4. Friction Law

[68] There are a variety of friction laws that are used; these include [*Rabinowicz et al.*, 1995] the following: (1) The static-dynamic law is of the Coulomb-Mohr or "freshman physics" type, in which there is a constant static coefficient of friction μ_s and a constant dynamic coefficient of sliding friction μ_d. Stick-slip behavior is obtained if $\mu_s > \mu_d$. (2) Velocity weakening is the friction law, used in the classic *Burridge and Knopoff* [1967] paper; it involves a static friction threshold, followed by a dependence on an inverse power of the slipping velocity. (3) The slip weakening law is similar to the static-dynamic law, but the friction weakens over a characteristic distance. (4) Rate and state friction law is a phenomenological law arising from laboratory experiments, in which a block slides over a surface, with occasional sudden changes in sliding velocity. After each change in sliding velocity it is observed that stress relaxes to a new value over some characteristic sliding distance. Conditions under which these friction laws are observed to have unstable sliding include an extremely stiff testing machine and clean sliding surfaces.

5.4.5. Imposed Randomness

[69] There are two principal types of imposed randomness: (1) Quenched randomness is represented as random variations from block to block in parameters such as spring constants and/or friction coefficients. (2) In annealed randomness, stress drops in the CA approach on a block during a slip event are randomly varied by adding a random undershoot or overshoot. A characteristic of all solutions is that, over at least a limited range, the slip events tend to have a power law frequency-area distribution, although true power law behavior is only observed in models with long-range interactions [*Ferguson et al.*, 1999; *Castellaro and Mulargia*, 2002]. An example is given in Figure 9. The number of slip events per time step with area A_e, N_e/N_0, is given as a function of A_e. In this simulation the cellular automata approach was used with static-dynamic friction. Results are given for stiffness $\beta = 30$, ratio of static to dynamic friction is 1.5, and grid sizes are $n \times n = 20 \times 20$, 30×30, 40×40, and 50×50. For stiff systems, large β, the entire grid of slider blocks is strongly correlated, and large events, including all blocks, occur regularly. These are the peaks at $A_e = 400$, 900, and 1600 illustrated in Figure 9.

6. STATISTICAL PHYSICS OF SLIDER BLOCK MODELS

6.1. Application to Earthquakes

[70] In the emerging picture of earthquake physics it has been shown that earthquakes can be regarded as generalized phase transitions [*Smalley et al.*, 1985; *Rundle*, 1989; *Main*, 1996]. There has been a lively debate about whether earthquakes are best represented by a second-order or first-order phase transition. However, recent results [*Rundle and Klein*, 1993, 1995b; *Rundle et al.*, 1997a, 1998; *Klein et al.*, 1997, 2000] are leading to the view that the first-order transition represents by far the richer physical picture, complete with predictions of

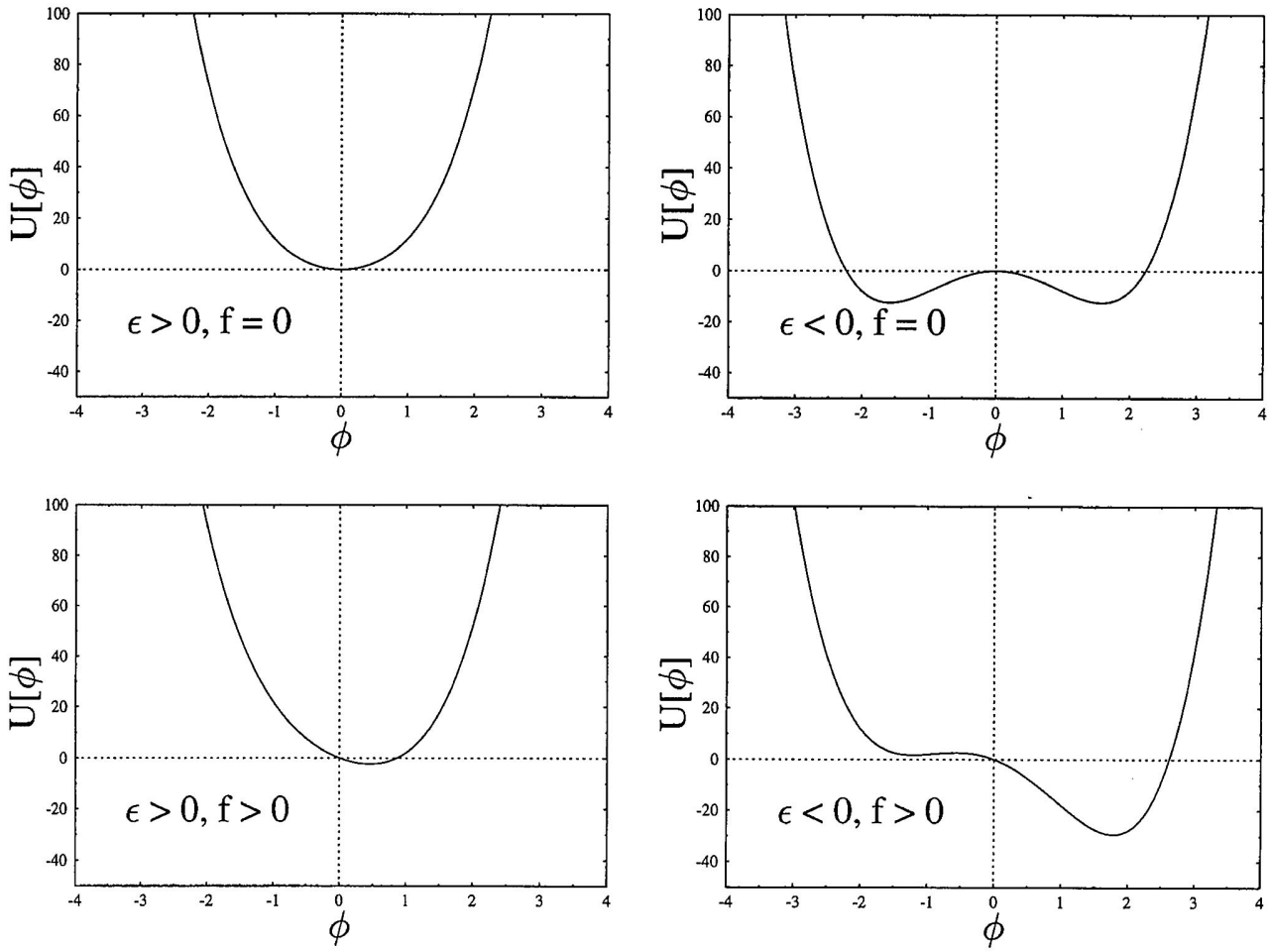

Figure 10. Potential energy U [ϕ] as a function of displacement ϕ as given by equation (19). (left) With ε $>$ 0, a single potential well. (right) With ε $<$ 0, two potential wells. With $f = 0$ the wells are equal. As f is increased, the left well becomes shallower, and the right well becomes deeper. The left well is a metastable state since it is not the state of minimum potential energy. As f is increased further, an inflection point occurs, and the left minimum disappears; this is the spinodal point.

scaling phenomena and space-time patterns that have been successfully tested by observations.

[71] In the first-order, phase-transition picture, plate tectonic forces drive a fault into a state of metastable equilibrium. Because the elastic interactions are long range [*Klein and Unger*, 1983; *Ray and Klein*, 1990], near mean field conditions prevail, and the fault can approach a near spinodal line [*Rundle and Klein*, 1993]. In fact, in the case of repeated earthquakes on a fault through time the system is regarded as residing permanently in the neighborhood of the spinodal line, executing a variety of fluctuations near the spinodal line through time [*Klein et al.*, 2000]. In this picture the order parameter for the fault can be regarded as either the stress, the slip, or the slip deficit, all of which change dramatically at the time of an earthquake on the fault.

6.2. Multistate System

[72] To make this discussion a bit more concrete and to provide a connection of the physics discussed in section 3 to slider blocks and earthquakes, consider the energy function $U[\phi]$, which is a function of the variable ϕ,

$$U[\phi] = \varepsilon\, \phi^2 + \alpha\, \phi^4 - f\, \phi \ . \qquad (19)$$

$U[\phi]$ is an example of a Ginzburg-Landau functional [*Ma*, 1976]. In a typical example, $U[\phi]$ is the potential energy associated with two particles separated by a distance ϕ, the constants ε and α represent the interparticle forces, and f is an applied force. Equations of the form of equation (19) have been used to describe systems with multiple possible states, in which sudden transitions between the states are possible. Typical dependencies of $U[\phi]$ on ϕ are given in Figure 10 for various values of the parameters. It can be seen from Figure 10 that the form of U changes depending upon the sign of α and ε and upon whether f is nonzero. In most physical systems, one would only be interested in conditions when $\alpha > 0$, because then U can be minimized for finite values of the variable ϕ. The control parameter f determines whether the function U is symmetric under a space reflection or not.

[73] As an example of a system that might be governed by an equation such as equation (19), consider the case of a block being pulled along a surface by a constant velocity driver connected to the block by a spring. If we consider U to represent the thermodynamic free energy of this system, then the system configuration point ϕ tends to evolve in such a way as to minimize U. Similarly, equilibrium is described by the following equation:

$$\frac{dU}{d\phi} = 2\,\varepsilon\,\phi + 4\,\alpha\,\phi^3 - f = 0\ , \qquad (20)$$

which is obtained by taking the derivative of equation (19) and which is a representation of the principle of minimum free energy.

[74] The situation is illustrated in Figure 10. The left plots, where $\varepsilon > 0$, can be considered to represent stable sliding of the block. Here there is only a single local potential well in U; thus a small force f produces a small shift of the stable point ϕ_0 corresponding to the minimum value of U. These equations describe a simple model of stable sliding.

[75] In the right plots of Figure 10, $\varepsilon < 0$, and there is a very different physical situation in which there are two locally stable (minimum energy) states ϕ_L and ϕ_R (left and right). If $f = 0$, the two local potential wells are at equal depth, and neither state of ϕ is preferred on the basis of the lowest potential energy. However, now consider the situation when $f > 0$, so that the right well has lower energy than the left well. As f is increased, the left well becomes shallower, and the right well becomes deeper. Between the left local minimum in U and the right local minimum in U, there is a local maximum of U, $\phi_{max} \approx 0$, a free energy barrier between the two local minima. The left local minimum has higher energy than the right local minimum; thus the left minimum ϕ_L is metastable, whereas the right minimum ϕ_R is the lowest energy state and is therefore stable. When f is increased further, an inflection point will occur, and the left minimum will disappear; this is the limit of metastability. For the slider block model this limiting value of f corresponds to the static coefficient of friction, and the block will suddenly slip, thus reducing f. The local maximum is correspondingly a state of locally unstable equilibrium. This model is therefore a candidate for a process of unstable stick slip: If the system configuration initially corresponds to the metastable state, as f increases, a sudden transition will occur at some point as the system configuration moves from the higher free energy, metastable well to the lower free energy, stable well. In doing so, the system point must pass over the local energy barrier near $\phi = 0$. In a more generic sense this process is called nucleation, and it corresponds to a first-order phase transition.

[76] The spinodal line is defined by the values of parameters α, ε, and f at which the energy barrier just disappears, and the function $U[\phi]$ has a point of inflection. The spinodal line represents the classical limit of stability of the system, since the disappearance of the energy barrier means that the system now has only one local minimum, the globally stable minimum, instead of two local minima. Therefore the transition from ϕ_L to ϕ_R with increasing f becomes inevitable.

[77] It is clearly desirable to extend the model described above, which is applicable to a single slider block, to a large array of slider blocks. A more general version of equation (20) that allows for both spatial and temporal fluctuations $\phi \Rightarrow \Phi\,(\mathbf{x}, t)$ is the time-dependent Ginzburg-Landau equation [*Haken*, 1983]:

$$T\,\frac{\partial \Phi}{\partial t} = R^2\,\nabla^2\Phi - 2\,\varepsilon\,\Phi - 4\,\alpha\,\Phi^3 + f\ . \qquad (21)$$

This equation arises in many branches of science when the effects of sudden (first order) transitions from one state to another are observed. In the case of earthquakes, for example, it is a simple representation for the physical situation of two media in contact at an irregular sliding surface, having bumps, divots, and asperities, in which $\Phi(\mathbf{x}, t)$ represents the difference between the displacement at point $\mathbf{x}$ and time t.

[78] Here the coefficient T is a characteristic time, and the coefficient R^2 of the new Laplacian term is the square of the range of interaction R, which physically represents the distance over which the effects of a fluctuation in $\Phi(\mathbf{x}, t)$ at $\mathbf{x}$ are directly communicated to physical variables such as the stress and slip that are located at another point $\mathbf{x}'$. Spatial and temporal variations in $\Phi(\mathbf{x}, t)$ are now possible.

6.3. Scaling

[79] Equation (21) allows us to demonstrate that scaling and power law statistical distributions are necessarily associated with second-order phase transitions. The basic idea is to scale equation (21) so that it is uniformly valid near possible phase transitions. The important control parameters in this process are ε and f, since the magnitude and sign of these parameters controls the form of $U[\Phi(\mathbf{x}, t)]$ and therefore the characteristics of the phase transition.

[80] Let us first set $f = 0$ and consider the necessary scaling of equation (21) in the vicinity of $\varepsilon = 0$. In order to do this we introduce the scaled nondimensional variables

$$\mathbf{x}' = \frac{\mathbf{x}}{\xi}\,, \quad t' = \frac{t}{\tau}\,, \quad \Phi' = \frac{\Phi}{\varepsilon^{1/2}}\ . \qquad (22)$$

Substitution of equation (22) into equation (21) taking $f = 0$ gives

$$\frac{\partial \Phi'}{\partial t'} = \nabla'^2\Phi' - 2\,\Phi' - 4\,\alpha\,\Phi'^3\ . \qquad (23)$$

On the basis of the scaling given in equation (22) we define a correlation length ξ and correlation time τ according to

$$\xi = \frac{R}{\varepsilon^{1/2}}, \qquad \tau = \frac{T}{\varepsilon} . \tag{24}$$

In the limit $\varepsilon \rightarrow 0$ the critical point, the correlation length, and time approach infinity with a power law scaling.

[81] Alternatively, we can set $\varepsilon = 0$ and consider the necessary scaling of equation (21) in the vicinity of $f = 0$. In order to do this we introduce the scaled nondimensional variables:

$$\mathbf{x}' = \frac{\mathbf{x}}{\xi}, \qquad t' = \frac{t}{\tau}, \qquad \Phi' = \frac{\Phi}{f^{1/3}} . \tag{25}$$

Substitution of equation (25) into equation (21) taking $\varepsilon = 0$ gives

$$\frac{\partial \Phi'}{\partial t'} = \nabla'^2 \Phi' - 4\,\alpha\,\Phi'^3 + 1 . \tag{26}$$

On the basis of the scaling given in equation (24) we define a correlation length ξ and correlation time τ according to

$$\xi = \frac{R}{f^{1/3}} \qquad \tau = \frac{T}{f^{2/3}} . \tag{27}$$

In the limit $f \rightarrow 0$ the critical point, the correlation length ξ, and correlation time τ again approach infinity with power law scaling.

[82] These values for (ε, f), i.e., (0, 0), define the Landau-Ginzburg "critical point." The control parameters (ε, f), which measure the proximity of the system to the critical point, are called "scaling fields." A unique property of such a critical point is that, independent of whether ε or f is the control parameter, one has a scaling relation for the length ξ in terms of one of the scaling fields, where ξ is the correlation length, because it sets the scale for the spatial fluctuations arising from the Laplacian term [*Stanley*, 1971; *Gunton and Droz*, 1983; *Binney et al.*, 1993]. Likewise τ is the correlation time, because it sets the timescale for fluctuations arising from the time derivative term.

[83] A more concrete connection between the physics of nucleation and critical phenomena and earthquakes was made by a model called the traveling density wave (TDW) model for earthquakes [*Rundle et al.*, 1996]. Here the equation analogous to equation (21) can be written as

$$T\frac{\partial \Phi}{\partial t} = -\{k_L\,\Phi + R^2\,\nabla^2\Phi + 2\gamma\,\kappa\,\sin[\kappa(\Phi + V\,t)]\}, \tag{28}$$

where the term $k_L\Phi$ has replaced f. The sine term is new and represents a periodic friction force. The system is driven at the plate velocity V by the sine term. In applications to real materials the sine term would presumably be replaced by a Fourier sum of terms. There might also be noise in the form of an additive random noise term, the two effects leading to a random, disordered pinning force representing friction between sliding surfaces [*Rundle et al.*, 1996].

[84] To understand the dynamics of equation (28), let us search for a solution $\Phi(\mathbf{x}, t) \rightarrow \phi(t)$ that is uniform in space (no spatial fluctuations) but varying in time. Then we have the following equation:

$$T\frac{d\phi}{dt} = -\{k_L\,\phi + 2\gamma\,\kappa\,\sin[\kappa(\phi + V\,t)]\} . \tag{29}$$

Corresponding to equation (29), there is also an energy function $U[\phi, t]$:

$$U[\phi, t] = \frac{1}{2}\,k_L\,\phi^2 - 2\gamma\,\cos[\kappa(\phi + V\,t)] . \tag{30}$$

Equation (29) is related to equation (30) via the principle of minimum energy in irreversible thermodynamics [*Rundle*, 1989]:

$$\frac{d\phi}{dt} = -\frac{\partial U[\phi, t]}{\partial \phi} . \tag{31}$$

[85] The physics of this model is illustrated in Figure 11, which again involves the idea of metastability and a spinodal line or limit of stability. If the parameter $\Lambda \equiv 2\gamma\,\kappa^2/k_L > 1$, we have the situation shown at the top of Figure 11; a metastable state is possible, and a recurring spinodal line appears. If $\Lambda < 1$, we have the situation at the bottom of Figure 11, where there is always only one time-dependent, stable state. The top plots represent the case of periodic stick-slip, whereas the bottom plots represent the case of stable sliding at variable speed.

[86] The k_L term in equation (29) is represented by a quadratic potential well $(1/2)k_L\phi^2$ that is periodically distorted by the leftward propagating cosine wave. The top right plot in Figure 11 illustrates how the plate motion V in equation (29) prepares the system for the next event by (1) taking the globally stable potential well just after the last event and moving the system configuration point into a state of metastable equilibrium and then (2) gradually reducing the energy barrier until the spinodal line is reached, eventually allowing the system to decay spontaneously during the unstable slip event. It can be seen from this discussion that between events, there is a period of time just after the last earthquake when there is only one globally stable system state. At a later time the globally stable state gradually transforms to a metastable state, at which three equilibrium points exist: one metastable state, one unstable state, and one globally stable state. Stick-slip sliding is only possible when the three solutions come into existence, since only then is a decay from a metastable equilibrium possible.

[87] The TDW model illustrates intermittent criticality [*Sammis et al.*, 1996]. The process of decay can be understood by an analysis of the solutions to equation (29), and, in particular, these solutions have a number of the scaling properties observed in nature, including Gutenberg-Richter scaling, Omori-type scaling, and so

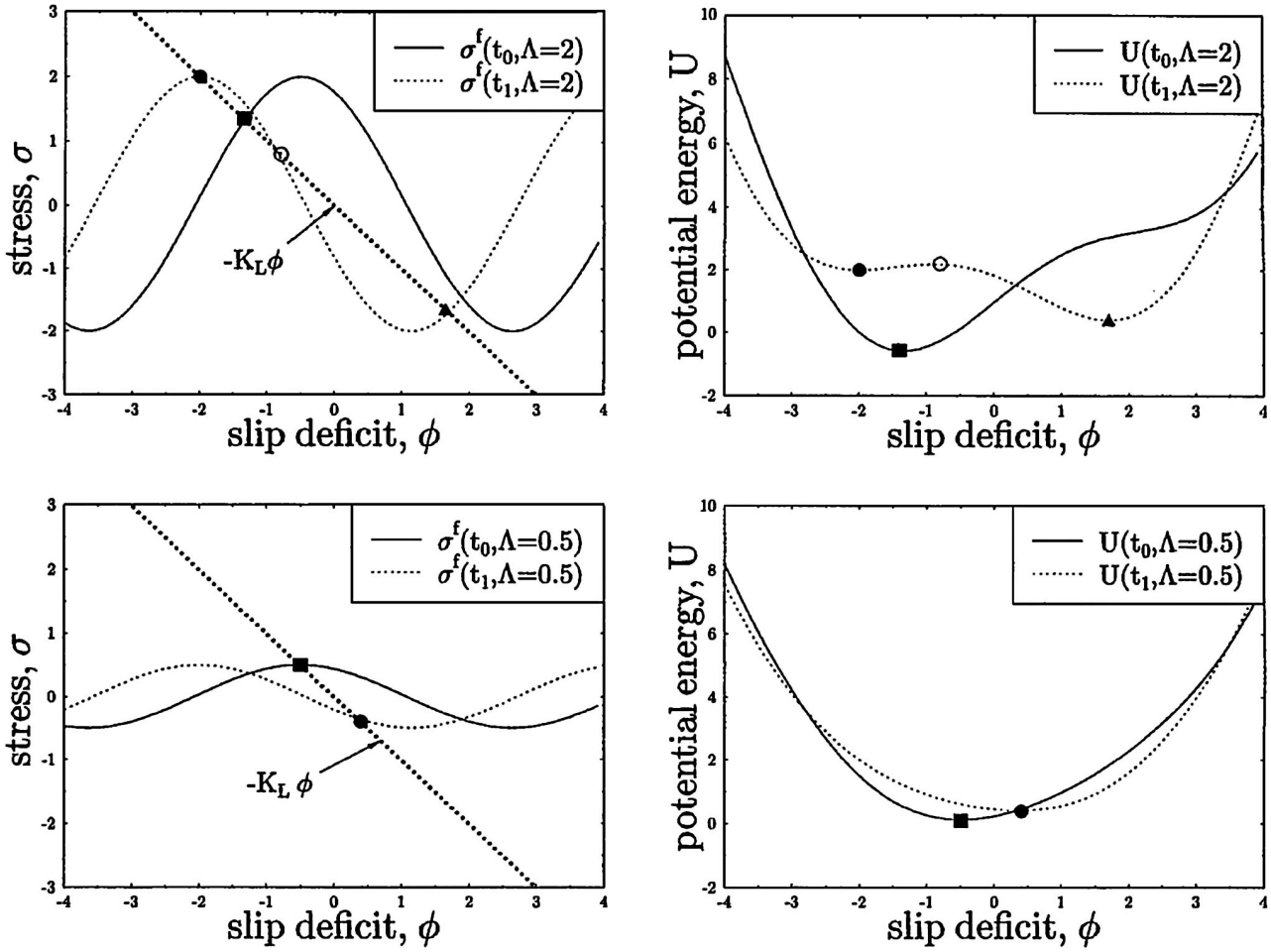

Figure 11. Traveling density wave model. (top) Plots with parameter $\Lambda = 2$ so that a spinodal exists (recurrent "brittle failure"). (bottom) Plots with $\Lambda = 0.5$ so that a spinodal does not exist (recurrent "ductile sliding"). (left) Stress σ as a function of slip deficit ϕ. (right) Energy U as a function of slip deficit ϕ.

forth [*Rundle et al.*, 1996, 1997a, 1997b]. The time interval $\delta t = t - t_{sp}$, during which the nucleation barrier disappears and the decay from the metastable state becomes inevitable, acts as a scaling field because it brings the system toward or away from the spinodal line. The latter acts as a critical point near which scaling occurs.

[88] The preevent and postevent fluctuations and the process of decay from metastability may be related to the underlying physical mechanisms behind the foreshock–main shock–aftershock sequence. Examples of our simulation results, together with real data from cycles of activity in the Mammoth Lakes, California, region, are shown in Figure 12. Similar cycles can be seen in other areas of the world [*Scholz*, 2002]. The simulation results were obtained on a lattice of size $64 \times 64 = 4096$ sites. The correlation length ξ [*Klein et al.*, 1996; *Rundle et al.*, 1997a, 1997b] varies inversely with the barrier height separating the stable and metastable states:

$$\xi \sim (k_L V|\delta t|)^{-1/4} . \qquad (32)$$

Equation (32) says that as the main shock time is approached, the correlation length grows. In the vicinity of the spinodal line the correlation length diverges as the inverse-fourth power of the barrier height rather than the inverse-half power encountered in equation (23). The description of this physical process closely resembles the "intermittent criticality" model proposed by *Sammis et al.* [1996] to explain the development and growth of correlations on an earthquake fault as the time of the main shock approaches. Corresponding changes in earthquake scaling during the foreshock and aftershock phases, consistent with the predictions of equation (32), have recently been observed by *Jaumé and Sykes* [1999] and *Bowman et al.* [1998]. We will thus be motivated to explore these similarities in detail to find out what observable properties should be reflected in seismicity distributions and clustering. Depending on the physical details of the configuration of the metastable well, this model may be associated either with quiescence (depressed foreshock activity), or with elevated precursory activity (enhanced foreshock activity).

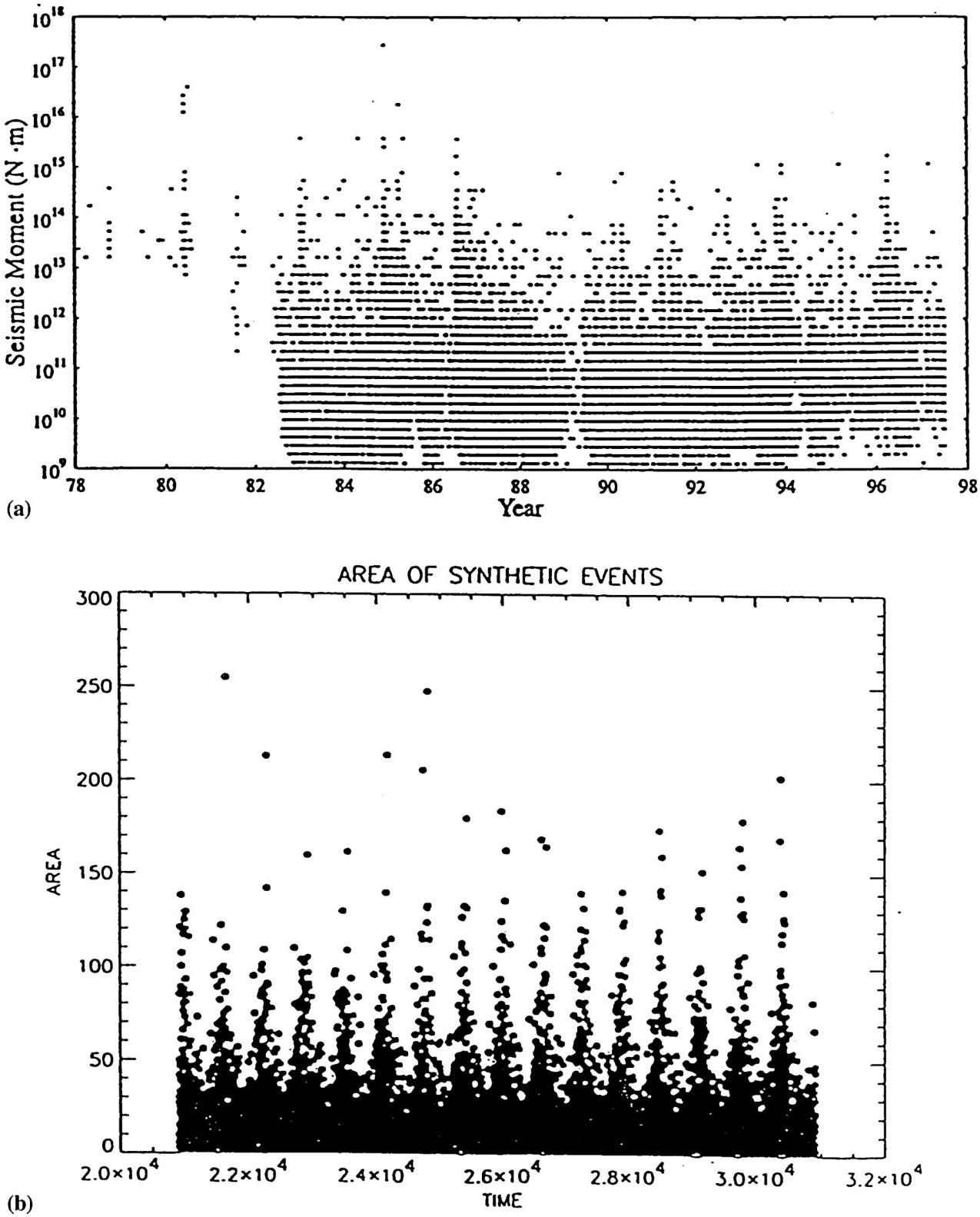

Figure 12. Cycles of earthquake activity (foreshock–main shock–aftershock events) from (a) Mammoth Lakes, California, and (b) traveling density wave simulations [after *Rundle et al.*, 1999].

7. EARTHQUAKE FORECASTING METHODS

[89] As discussed in sections 1 and 2, it is generally accepted that earthquakes are a chaotic phenomenon. Thus, as in the case of weather forecasting, earthquake forecasting must be considered on a statistical basis. However, there are no widely accepted earthquake forecasting algorithms currently available. A fundamental

question is whether patterns of seismicity can be used to forecast future earthquakes. Promising results suggesting that this may be possible have recently been obtained. The data on accelerated moment release given in section 2.3 certainly indicate that there may be "action at a distance" prior to at least some earthquakes. This "action at a distance" may be the physics underlying the earthquake prediction algorithms developed at the International Institute for the Theory of Earthquake Prediction and Theoretical Geophysics in Moscow under the direction of academician V. I. Keilis-Borok. This approach is based on pattern recognition of distributed regional seismicity [*Keilis-Borok*, 1990; *Keilis-Borok and Rotwain*, 1990; *Keilis-Borok and Kossobokov*, 1990; *Keilis-Borok and Soloviev*, 2003]. Premonitory seismicity patterns were found for strong earthquakes in California and Nevada (algorithm "CN") and for earthquakes $m >$ 8.0 worldwide (algorithm "M8"). When a threshold of the anomalous behavior was reached, a warning of the time of increased probability (TIP) of an earthquake was issued. Successful TIPs were issued prior to 42 of 47 events. TIPs were released prior to the Armenian earthquake on 7 December 1988 and prior to the Loma Prieta earthquake on 17 October 1989. This approach is certainly not without its critics. Independent studies have established the validity of the TIP for the Loma Prieta earthquake; however, the occurrence of recognizable precursory patterns prior to the Landers earthquake is questionable. Also, the statistical significance of the size and time intervals of warnings in active seismic areas has been questioned. Nevertheless, seismic activation prior to a major earthquake certainly appears to be one of the most promising approaches to earthquake forecasting.

[90] An alternative pattern informatics (PI) approach to earthquake forecasting has been proposed by *Rundle et al.* [2000d, 2002] and *Tiampo et al.* [2002a, 2002c]. This approach is based on the strong space-time correlations that are responsible for the cooperative behavior of driven threshold systems such as the TDW model described in section 6.3. The correlations arise both from the threshold dynamics, as well as from the mean field (long range) nature of the interactions. Driven threshold systems can be considered to be examples of phase dynamical systems [*Mori and Kuramoto*, 1997] when the rate of driving is constant, so that the integrated stress dissipation or firing rate over all sites is nearly constant, with the exception of small fluctuations.

[91] In threshold systems such as earthquake faults, the stress is typically supplied at a steady rate but is dissipated episodically by means of the earthquakes. Owing to the mean field nature of both the simulated and real threshold systems it is found that as the size of the system N is increased, the amplitude of the "small fluctuations" decreases roughly as $1/\sqrt{N}$.

[92] Using both simulations and observed earthquake data, *Tiampo et al.* [2000, 2002c] and *Rundle et al.* [2000d, 2002] have shown that the space-time patterns of threshold events (earthquakes) can be represented by a time-dependent system state vector in a Hilbert space. The length of the state vector represents the average temporal frequency of events throughout the region and is closely related to the rate $f[\sigma, V]$ at which stress is dissipated. It can be deduced that the information about space-time fluctuations in the system state is represented solely by the phase angle of the state vector hence the term "phase dynamics." Changes in the norm of the state vector represent only random fluctuations and can for the most part be removed by requiring the system state vector to have a constant norm.

[93] This PI approach is best illustrated using a specific example. *Tiampo et al.* [2000, 2002b] analyzed data from southern California since 1932 between 32° and 37° north latitude and 238° to 245° east longitude. The surface area was divided into $N = 3162$, square boxes with size $L_{CG} = 0.1° \sim 11$ km, corresponding roughly to the linear size of a magnitude $m \sim 6$ earthquake. The standard online data set available through the web site maintained by the SCEC (the SCSN catalog) was used. This data set includes all instrumentally recorded earthquakes in southern California beginning at time $t_0 = 1$ January 1932 and extending to the present. For this region, earthquakes with magnitude greater than $m_c = 3$ are typically used to insure catalog completeness since 1932. The idea is to use small events having scales $\lambda < L_{CG}$ to forecast the occurrence of large events having scales $\lambda > L_{CG}$.

[94] The seismic intensity in box i is defined to be the total number, $N(\mathbf{x}_i, t_b, t)$, of earthquakes in the box during the time period t_b to t with magnitudes greater than m_c. For each box an activity rate function $S(\mathbf{x}_i, t_b, t)$ is defined to be the average rate of occurrence of earthquakes in box i during the period t_b to t. That is,

$$S(\mathbf{x}_i, t_b, t) = \frac{N(\mathbf{x}_i, t_b, t)}{t - t_b} \ . \tag{33}$$

The normalized activity rate function is found by subtracting the spatial mean for all boxes and dividing by the spatial standard deviation

$$\hat{S}(\mathbf{x}_i, t_b, t) = \frac{S(\mathbf{x}_i, t_b, t) - \frac{1}{N}\sum_j S(\mathbf{x}_j, t_b, t)}{\left\{\frac{1}{N}\sum_j \left[S(\mathbf{x}_j, t_b, t) - \frac{1}{N}\sum_k S(\mathbf{x}_k, t_b, t)\right]^2\right\}^{1/2}} \ . \tag{34}$$

The change in the normalized activity rate function for the forecast time period t_1 to t_2 is found by subtracting the normalized activity rate function for the time period t_b to t_1 from the normalized activity rate function for the time period t_b to t_2

$$\Delta\hat{S}(\mathbf{x}_i, t_b, t_1, t_2) = \hat{S}(\mathbf{x}_i, t_b, t_2) - \hat{S}(\mathbf{x}_i, t_b, t_1) \ . \tag{35}$$

Changes in the normalized activity rate function are then obtained for a sequence of values of t_b taken at yearly intervals from t_0 to $t_1 - 1$. These changes are then averaged to give the mean normalized change in activity

$$\Delta s(\mathbf{x}_i, t_0, t_1, t_2) = \frac{1}{t_1 - 1 - t_0} \sum_{t_b=t_0}^{t_1-1} \Delta\hat{S}(\mathbf{x}_i, t_b, t_1, t_2) \quad . \tag{36}$$

Finally, we introduce a probability of change of activity in a box relative to the background; this is given by the difference between the square of the mean normalized change in activity for a box and its spacial mean:

$$\Delta P(\mathbf{x}_i, t_0, t_1, t_2) = [\Delta s(\mathbf{x}_i, t_0, t_1, t_2)]^2 - \frac{1}{N} \sum_j [\Delta s(\mathbf{x}_j, t_0, t_1, t_2)]^2 \quad . \tag{37}$$

Because the $\Delta s(\mathbf{x}_i, t_0, t_1, t_2)$ are squared, the probability is a measure of both seismic activation and seismic quiescence. The use of the ΔP to forecast earthquakes is referred to as the pattern informatics method.

[95] We will now apply the PI method to southern California. The distribution of relative seismic intensities for southern California for the period 1932–1991 are given in Figure 13a. The relative intensity is defined to be the logarithm of the ratio of $N(\mathbf{x}_i, t_0, t_1)/N(\mathbf{x}_i, t_0, t_1)_{\max}$, where $N(\mathbf{x}_i, t_0, t_1)$ is the number of earthquakes in box i during the period t_0 = 1 January 1932 and t_1 = 31 December 1991 and $N(\mathbf{x}_i, t_0, t_1)_{\max}$ is the largest value of $N(\mathbf{x}_i, t_0, t_1)$.

[96] A PI method forecast of earthquake occurrence in this region is given in Figure 13b. In applying the method to the $N = 3162$ $0.1° \times 0.1°$ boxes with $m_c = 3.0$, the times used were t_0 = 1 January 1932, t_1 = 1 January 1978, and t_2 = 31 December 1991. This was meant to be a retrospective forecast for the period 1992–2002. Relative values of the probability of activity are given in the form $\log_{10}$ $(P_j/\Delta P_{j\max})$. The color-coded anomalies are shown in Figure 13b. Note that only positive values of $\log_{10}$ $(\Delta P_j/\Delta P_{j\max})$ are given. Thus the color-coded regions represent regions of anomalously high seismic activation or high seismic quiescence. Note that no data were used in the shaded anomalies of Figure 13b from the time after 31 December 1991, 6 months prior to the 27 June 1992 $m \sim 7.3$ Landers earthquake (34°13′N latitude, 116°26′W longitude). Earthquakes with $m >$ 5.0 that occurred during the period 1978–1991 are shown as inverted triangles. Earthquakes with $m > 5.0$ that have occurred since 1991 are shown as circles.

[97] Visual inspection of Figure 13b shows that the retrospective forecast is reasonably successful, but rigorous statistical testing is needed. *Tiampo et al.* [2000, 2002b] used two types of null hypotheses to test the forecast in Figure 13b. (1) Thousands of randomized earthquake catalogs were generated from the observed catalog by using the same location and total number of events but assigning each event a random occurrence time from a uniform probability distribution over the years 1932–1991. Randomizing the catalog in this way destroyed whatever coherent space-time structure may have existed in the data. These random catalogs were used to construct a set of null hypotheses, since any forecast method using such a catalog cannot, by definition, produce useful information. (2) For the second null hypothesis the seismic intensity data in Figure 13a was used directly as a probability density as has been proposed in the literature [*Kagan and Jackson*, 2000] for the standard null hypothesis.

[98] A maximum likelihood test [*Gross and Rundle*, 1998; *Bevington and Robinson*, 1992; *Kagan and Jackson*, 2000; *Tiampo et al.*, 2002a] was used to evaluate the accuracy with which probability measure ΔP_i can forecast "future" ($t > t_2$) "large" ($m \geq 5.0$) events, relative to forecasts from the null hypotheses. The likelihood $\mathcal{L}$ is a probability measure that can be used to assess the utility of one forecast measure over another. Typically, one computes $\log_{10}(\mathcal{L})$ for the proposed forecast measure $\mathcal{L}$ and compares that to the likelihood measure $\mathcal{L}_N$ for a representative null hypothesis. The ratio of these two values then yields information about which measure is more accurate in forecasting future events.

[99] Figure 13c shows computations of (1) $\log_{10}(\mathcal{L})$ for 500 random catalogs of the first type (histogram), (2) $\log_{10}(\mathcal{L})$ for the seismic intensity map in Figure 13a (vertical dashed-dotted line), and (3) $\log_{10}(\mathcal{L})$ for the forecast of Figure 13b (dashed line). Since larger values of $\log_{10}(\mathcal{L})$ indicate a more successful hypothesis, the logical conclusion is that the method has forecasting skill.

[100] The true test of any earthquake forecasting algorithm is to make a future forecast that proves correct. *Tiampo et al.* [2002a] and *Rundle et al.* [2002] did this for the period 2000–2010. This forecast is reproduced in Figure 14. Values of $\log_{10}(\Delta P_j/\Delta P_{j\max})$ are given using the same color code as in Figure 13b. For this forecast the times used were t_0 = 1 January 1932, t_1 = 1 January 1990, and t_2 = 31 December 1999. Also shown in Figure 14 are events with $m > 5.0$ that took place during the period 1990–1999.

[101] The success rate of this method of forecasting has been encouraging. A number of events were coincident, within the ±11 km margin of error (the coarse graining box size), with the forecasts, in that the large earthquakes occurred in areas predicted by the method to have a rapidly increasing probability of an event. These events (SCSN catalog) included the m = 5.1 Big Bear I event of 10 February 2001 (event 1, Figure 14); the m = 5.1 Anza event of 31 October 2001 (event 2, Figure 14); the m = 5.7 Baja event of 22 February 2002 (event 3, Figure 14); the m = 4.9 (first reported at m = 5.2) Gilroy event of 13 May 2002 (event 4, Figure 14); and the m = 5.4 Big Bear II event of 22 February 2003 (event 5, Figure 14). Of these events the first (Big Bear I) occurred after the research [*Rundle et al.*, 2002] had

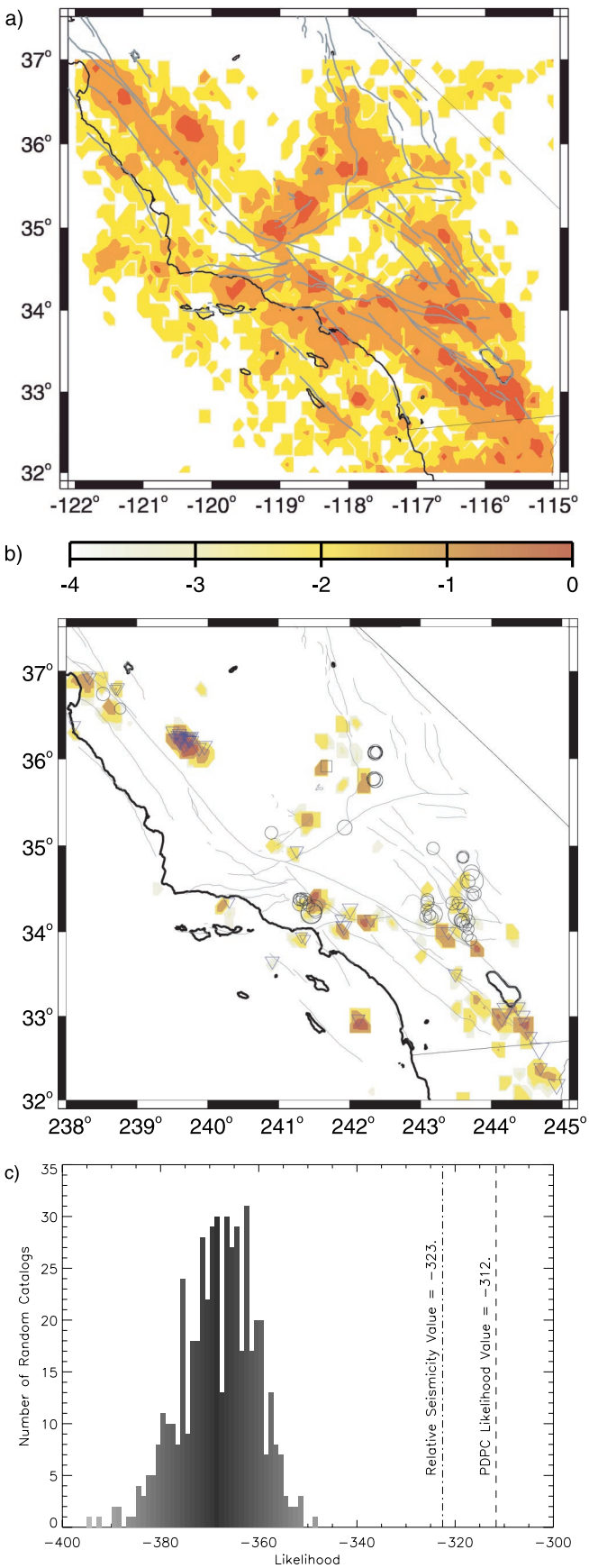

been completed (January 2001); the second (Anza) occurred after the paper was in press (June 2001); and events 3–5 all occurred after the publication of the article by *Rundle et al.* [2002] on 19 February 2002.

8. DISCUSSION

[102] This review describes recently developed approaches to understanding earthquake physics based on applying statistical physics to observed data and numerical simulations of earthquake processes. Earlier approaches emphasized either geologic investigations and mapping or the application of continuum methods developed in engineering, including fields such as elasticity, viscoelasticity, plasticity, fluid mechanics, and friction. The statistical physics approach differs from the earlier approaches by its emphasis on the treatment of earthquake faults and fault systems as high-dimensional dynamical systems characterized by a wide range of scales in both space and time. Examples of these scales can be seen in the fractal topology of fault systems, in the linearity of the Gutenberg-Richter magnitude-frequency relation, and in other observed statistics of earthquakes, including the modified Omori's aftershock relation and the Bufe-Varnes law for precursory activation.

[103] We have also described a variety of models, together with their analysis by statistical mechanical methods. Many of these models have been used to construct numerical simulations of earthquake physics, a number of which have used a cellular automaton approach. The first successful example of this class of models was the Burridge-Knopoff slider block model [*Burridge and Knopoff*, 1967], which used massive blocks leading to a set of differential equations based on Newton's second law. The first cellular automaton version of the Burridge-Knopoff slider block model was published by *Rundle and Jackson* [1977] and also included an

Figure 13. (a) Relative seismic intensities $\log_{10}[N(x_i, t_0, t_1)/N(x_i, t_0, t_1)_{max}]$ for southern California for the period 1932–1991 using the color code below Figure 13. (b) A retrospective forecast of earthquakes for the period 1992–2002 using the PI forecasting methodology. Relative probabilities for activity $\log_{10}(\Delta P/\Delta P_{max})$ are given for southern California using the color code above Figure 13. The times used were t_0 = 1 January 1932, t_1 = 1 January 1978, and t_2 = 31 December 1991. Earthquakes that occurred between 1978 and 1991 are shown as inverted triangles (smallest triangles $5.0 < m \leq 6.0$, intermediate triangles $6.0 < m \leq 7.0$, and largest triangles $m > 7.0$). Earthquakes that have occurred since 1991 are shown as circles (smallest circles $5.0 < m \leq 6.0$, intermediate circles $6.0 < m \leq 7.0$, and largest circles $m > 7.0$). (c) Likelihood ($\log_{10}\mathcal{L}$) values for 500 randomized test catalogs (histogram), intensity map in Figure 13a used as a forecast map (left vertical dashed-dotted line), and PI method from Figure 13b (right vertical dashed line). Larger relative likelihood values represent more probable forecast models.

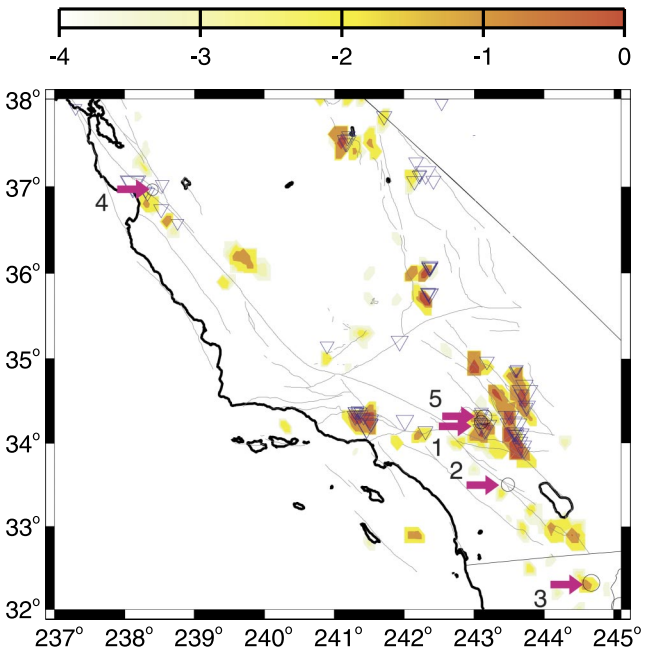

Figure 14. Pattern informatics method forecast for southern California for the period 2000–2010 [*Tiampo et al.*, 2002a; *Rundle et al.*, 2002]. Relative probabilities $\log_{10}(\Delta P/\Delta P_{max})$ are given using the color code at the top of Figure 14. The times used were t_0 = 1 January 1932, t_1 = 1 January 1990, and t_2 = 31 December 1999. Earthquakes with $m > 5.0$ that took place during 1990–1999 are shown as inverted triangles. Circles represent events with magnitude $m > 5.0$ that have occurred so far during the time period of the forecast.

analysis of earthquake physics based on a friction law characterized by time-dependent weakening.

8.1. Statistical Physics Applied to Fracture

[104] The statistical physics approach considers an earthquake to be a type of generalized phase transition. While some researchers have stressed the analogy of earthquakes to second-order phase transitions ("critical point model for earthquakes"), more recent work indicates that models based on nucleation and first-order phase transitions are probably more applicable. Both approaches lead to scaling laws or power law distributions for the dynamical variables. Second-order transitions demonstrate scaling near a critical point, whereas first-order transitions demonstrate scaling when the range of interaction is large (mean field condition), as is the case with elastic interactions. In first-order transitions the mean field condition allows the spinodal line, or classical limit of stability, to be approached during the transition process. The spinodal line behaves as a line of critical points, at which scaling laws with well-defined scaling exponents are seen.

[105] Brittle fracture, a process that is closely associated with earthquakes, is another example of a process that can be modeled by first-order phase transitions. The nucleation and coalescence of microcracks in brittle failure is analogous to the homogeneous nucleation of bubbles in a superheated liquid. A solid stressed above the yield stress is then considered to be in a metastable regime similar to that of the superheated liquid. The explosive homogeneous nucleation of bubbles in a superheated liquid occurs adjacent to the spinodal line, which is the limit of allowed superheating. Phase changes near a spinodal line have many of the scaling aspects of a second-order transition near the critical point but with different scaling exponents in general. Thus it appears reasonable to argue that the generation and coalescence of microcracks prior to material fracture is very similar to the homogeneous and/or heterogeneous nucleation of bubbles prior to the liquid-to-gas phase change in a superheated liquid.

8.2. Thermodynamic Variables

[106] Temperature plays an essential role in almost all applications of statistical physics. Thermal fluctuations are directly associated with the approach to a critical point or a phase change. These fluctuations are responsible for the homogeneous nucleation of a superheated liquid near a spinodal line.

[107] In the analogy between a phase change and brittle fracture it is clearly appropriate to associate stress with pressure and strain with specific volume (density). However, what about temperature? Experimental results are ambiguous. However, there is considerable evidence that fluctuations in stress (elastic vibrations) associated with microcracking play a role in brittle fracture that is analogous to the fluctuations in pressure caused by thermal fluctuations in a classical phase change.

8.3. Earthquake Nesting

[108] A fundamental question in earthquake physics is whether earthquakes are scale invariant. Is a magnitude m = 2.0 the same as a magnitude m = 4.0 is the same as a magnitude m = 6.0 is the same as a magnitude m = 8.0? Observations of seismic activation suggests it occurs for both large and small earthquakes. Increased numbers of earthquakes of magnitude 4 precede a 5.5 earthquake, increased numbers of earthquakes of magnitude 5.5 precede a 7.0 earthquake, and increased numbers of earthquakes of magnitude 7 precede an 8.5 earthquake. On the basis of results given in section 2.3, seismic activation occurred prior to the m = 7.5 Kern County earthquake, the m = 7.3 Landers earthquake, and the m = 6.7 Northridge earthquake.

8.4. Statistical Physics Models

[109] A number of models have been introduced in the past 15 years that exhibit the repetitive avalanche behavior and the power law scaling associated with fault systems. The model most closely associated with fault systems is the slider block model. The movement of the blocks over a surface takes place in slip events. These events scale in a manner similar to actual fault ruptures.

[110] Extensive studies of slider block models show that they exhibit a range of behaviors that commonly occur in statistical physics. The distribution of energies in the springs becomes thermalized and exhibits a Maxwell-Boltzmann distribution in many cases [*Rundle et al.*, 1995].

8.5. Earthquake Forecasting and Earthquake Patterns

[111] Statistical physics leads, in a natural way, to the development of methods for defining space-time patterns of seismicity. These methods can be used to determine whether there are systematic patterns of seismicity that might be precursors to future large earthquakes. Seismic activation, as proposed by *Bufe and Varnes* [1993], has now been recognized to have occurred for a significant number of earthquakes with a wide range of magnitudes (see Figure 2). Precursory quiescence, while more difficult to define and observe, may also occur: The power law increase in Benioff strain does not occur (or cannot be recognized) for all earthquakes. Studies of seismic activation to date have been largely retrospective, and forecasting and prediction of future large earthquakes based on pattern analysis methods is only just beginning.

[112] The Russian group, under the direction of V. I. Keilis-Borok, has developed a number of intermediate-term earthquake prediction algorithms based on pattern-recognition techniques [*Keilis-Borok and Soloviev*, 2003]. Regular earthquake "alarms" (Times of Increased Probability, or "TIPs") are issued. There have been two claims of success with this methodology, the 1988 Armenian earthquake and the 1989 Loma Prieta, California, earthquake. However, a number of relatively large earthquakes have not been predicted or forecast, and the approach is mired in controversy. A key element in these algorithms is a precursory increase in seismic activity over areas similar in size to the recognized patterns of seismic activation.

[113] Another, more recent approach to earthquake forecasting using Pattern Informatics (PI) was proposed by the Colorado group [*Rundle et al*, 2002; *Tiampo et al.*, 2002b, 2002c]. This approach, which does not rely on fitting any model parameters to training data, is based instead on ideas about phase dynamical systems. Classical examples of phase dynamics include fluid systems, reaction-diffusion systems, and in general, any dissipative system in which a phase can be defined [*Mori and Kuramoto*, 1998]. Here a probability for future large events can be computed from the data itself, without reference to any model. In this method, the migration of the smallest earthquakes from one spatial region to the next through time is used as an indicator for future activity of the largest events. Maps can be computed that forecast the locations and maximum magnitudes of the largest future events. A map of this type was published by *Rundle et al.* [2002] and *Tiampo et al.* [2002a]. Three earthquakes with magnitude $m > 5.0$ have occurred since publication of the first paper on February 19, 2002, and all three events have correctly fallen into the forecast regions (see Figure 14), thereby indicating that the method may have considerable promise.

9. CONCLUSION

[114] We have argued that earthquake fault systems represent a class of driven nonlinear dynamical systems characterized by a wide range of scales in both space and time, from centimeters to thousands of kilometers, and from seconds to many thousands of years. Patterns of behavior in high-dimensional natural systems are usually chaotic and complex. In most cases, it is difficult or impossible to directly observe the current state of the system, or to have detailed knowledge of the dynamics by which the system is evolving. The nonlinearity in the dynamics usually leads to strong couplings between the various space and timescales, so that activity on large space and long timescales can have dramatic impacts on the events that happen on small space and short timescales, and vice-versa. Observations of natural systems may have only limited utility in forecasting or extrapolating the future evolution of the system, since such observations are taken over a very limited range of scales, and are necessarily incomplete. A comprehensive understanding of the nonlinear dynamics of earthquake fault systems can only be developed by supplementing observations with a sophisticated program of numerical simulation, leading to the development of theoretical insights and results that can then be applied to the natural system. Simulations have the distinct advantages that 1) the effects of multiple scales in space and time can be examined, even those much larger and longer than human dimensions; 2) a variety of nonlinear dynamical processes can be proposed, and their effects determined, as candidates for the unobservable dynamics that characterize the natural system; and 3) data can be assimilated into the simulations using well-understood techniques, enabling the rigorous evaluation of the importance of particular data and leading to the development of organized data collection programs. Here we have summarized results from a new generation of earthquake fault system simulations, together with newly-developed analytical techniques for these fundamentally high-dimensional systems that arise from a statistical physics point of view. Note that the analytical techniques are fundamental and are already being applied to the understanding of other high-dimensional nonlinear systems, including neural networks, glass transitions, driven foams, semiconductors, and superconductors. The research we describe demonstrates the usefulness of even simple high-dimensional models such as slider block systems with cellular automaton dynamics, forest fire models, and percolation models. Even at this early stage, the models are predicting results that are being confirmed by new observations. An example is the time variation in regional earthquake magnitude-fre-

quency distribution prior to large earthquakes. A new state vector analysis technique for regional seismicity observations is another example that shows considerable promise as an intermediate-term earthquake forecasting tool.

NOTATION

a measure of the regional level of seismicity.
A rupture area.
A_e area of slip events.
A_{F} area of a burning cluster.
b "b value."
B constant in equation (7).
C constant in equation (3).
c specific heat.
D fractal dimension.
e_i seismic energy release of ith earthquake.
E_0 Young's modulus.
f force.
f_s sparking frequency.
F compressive force.
h magnetic field.
H hazard rate.
k_{C} connecting spring constant.
k_{L} loader plate spring constant.
L length of sample.
L_{CG} size of square box.
$\mathcal{L}$ likelihood probability measure.
m magnitude of earthquake.
m_c magnitude cutoff.
m mass of a slider block.
M magnetization.
N number of events.
N_{as} number of aftershocks.
N_e numbers of slip events.
N_F number of fires.
N_{GR} cumulative number of earthquakes.
p exponent in the Omori's law.
p probability.
P pressure.
P_c critical pressure.
P_f failure pressure.
P_y yield pressure.
ΔP change in probability for seismic activity.
q lattice coordination number.
R range of interaction.
s exponent in equation (7).
$\bar{s}$ mean value of s.
S activity rate function.
$\hat{S}$ normalized activity rate function.
Δs mean normalized activity rate
t time.
t_0, t_1 constants in the Omori's law.
t_0, t_1, t_2, t_b reference dates.
t_f time to failure.
t_d characteristic damage time.
t_{sp} time at which the spinodal point is reached.
δt time interval.
Δt nondimensional time.
T characteristic time.
T temperature.
T_c temperature at the critical point.
U energy potential.
v specific volume.
v_c critical specific volume.
V driver plate velocity.
z dynamic exponent.
$\mathbf{x}$ spatial coordinate.
α damage variable.
α constant.
β stiffness of the system.
γ exponent in equation (3).
γ parameter in equation (28).
Γ Ginzburg criterion.
ε constant in equation (19).
ε_{B} cumulative Benioff strain.
ε_0 cumulative Benioff strain at $\Delta t = 0$.
ϵ strain.
ϵ_y yield strain.
κ parameter in equation (28).
λ length scale.
Λ parameter in section 6.3.
μ_d coefficient of dynamic friction.
μ_s coefficient of static friction.
ϕ order parameter (slip deficit).
$\phi_L, \phi_R, \phi_{\max}$ extremum values of ϕ.
Φ slip deficit.
τ shear stress.
τ critical slowing down.
σ stress.
σ_N normal stress.
σ_y yield stress.
ρ exponent in equation (18).
ρ density.
ρ_c density at the critical point.
ρ_{gas} density of a gas phase.
ξ correlation length.

[115] **ACKNOWLEDGMENTS.** This work has been supported by NASA/JPL grant 1247848 and U.S. DOE grant DE-FG03-03ER15380 (JBR, DLT, and RS) and by U.S. DOE/OBES grant DE-FG02-95ER14498 and W-7405-ENG-6 at LANL (WK). We would like to thank Kristy Tiampo for her many contributions to this work. We would also like to thank Yehuda Ben-Zion, Murray Gell-Mann, James Holliday, David D. Jackson, Tom Jordan, Vladimir Keilis-Borok, Vladimir Kossobokov, Bernard Minster, and Frank Press for many helpful conversations.

[116] Thomas Torgersen is the Editor responsible for this

paper. He thanks two technical reviewers and one cross-disciplinary reviewer.

REFERENCES

Aki, K., A probabilistic synthesis of precursory phenomena, in *Earthquake Prediction: An International Review*, *Maurice Ewing Ser.*, vol. 4, edited by D. W. Simpson and P. G. Richards, pp. 566–574, AGU, Washington, D. C., 1981.

Anghel, M., W. Klein, J. B. Rundle, and J. S. Sá Martins, Scaling in a cellular automaton model of earthquake faults, *Phys. Rev. E*, in press, 2003.

Bak, P., C. Tang, and K. Weisenfeld, Self-organized criticality, *Phys. Rev. A*, *38*, 364–374, 1988.

Bak, P., K. Chen, and C. Tang, A forest-fire model and some thoughts on turbulence, *Phys. Lett. A*, *147*, 297–300, 1992.

Ball, P., *The Self-Made Tapestry*, Oxford Univ. Press, New York, 1999.

Ben-Zion, Y., and V. Lyakhovsky, Accelerated seismic release and related aspects of seismicity patterns on earthquake faults, *Pure Appl. Geophys.*, *159*, 2385–2412, 2002.

Ben-Zion, Y., and C. G. Sammis, Characterization of fault zones, *Pure Appl. Geophys.*, *160*, 677–715, 2003.

Bevington, P. R., and D. K. Robinson, *Data Reduction and Error Analysis for the Physical Sciences*, McGraw-Hill, New York, 1992.

Binder, K., and D. W. Heermann, *Monte Carlo Simulation in Statistical Physics, An Introduction*, 3rd ed., *Springer Ser. Solid State Sci.,*, vol. 80, 150 pp., Spring-Verlag, New York, 1997.

Binney, J. J., N. J. Dowrick, A. J. Fisher, and M. E. J. Newman, *The Theory of Critical Phenomena*, Oxford Univ. Press, New York, 1993.

Bowman, D. D., and G. C. P. King, Accelerating seismicity and stress accumulation before large earthquakes, *Geophys. Res. Lett.*, *28*, 4039–4042, 2001.

Bowman, D. D., G. Ouillon, C. G. Sammis, A. Sornette, and D. Sornette, An observational test of the critical earthquake concept, *J. Geophys. Res.*, *103*, 24,359–24,372, 1998.

Brehm, D. J., and L. W. Braile, Intermediate-term earthquake prediction using precursory events in the New Madrid seismic zone, *Bull. Seismol. Soc. Am.*, *88*, 564–580, 1998.

Brehm, D. J., and L. W. Braile, Intermediate-term earthquake prediction using the modified time-to-failure method in southern California, *Bull. Seismol. Soc. Am.*, *89*, 275–293, 1999a.

Brehm, D. J., and L. W. Braile, Refinement of the modified time-to-failure method for intermidiate-term earthquake prediction, *J. Seismol.*, *3*, 121–138, 1999b.

Buchel, A., and J. P. Sethna, Statistical mechanics of cracks: Fluctuations, breakdown, and asymptotics of elastic theory, *Phys. Rev. E*, *55*, 7669–7690, 1997.

Bufe, C. G., and D. J. Varnes, Predictive modeling of the seismic cycle of the greater San Francisco Bay region, *J. Geophys. Res.*, *98*, 9871–9883, 1993.

Bufe, C. G., S. P. Nishenko, and D. J. Varnes, Seismicity trends and potential for large earthquakes in the Alaska-Aleutian region, *Pure Appl. Geophys.*, *142*, 83–99, 1994.

Burridge, R., and L. Knopoff, Model and theoretical seismicity, *Bull. Seismol. Soc. Am.*, *58*, 341–371, 1967.

Carlson, J. M., J. S. Langer, and B. E. Shaw, Dynamics of earthquake faults, *Rev. Mod. Phys.*, *66*, 657–670, 1994.

Castellaro, S., and F. Mulargia, What criticality in cellular automata models of earthquakes?, *Geophys. J. Int.*, *150*, 483–493, 2002.

Ciliberto, S., A. Guarino, and R. Scorretti, The effect of disorder on the fracture nucleation process, *Physica D*, *158*, 83–104, 2001.

Coleman, B. D., Time dependence of mechanical breakdown phenomena, *J. Appl. Phys.*, *27*, 862–866, 1956.

Coleman, B. D., Statistics and time dependence of mechanical breakdown in fibers, *J. Appl. Phys.*, *29*, 968–983, 1958.

Curtin, W. A., Theory of mechanical properties of ceramic-matrix composites, *J. Am. Ceram. Soc.*, *74*, 2837–2845, 1991.

Das, S., and C. H. Scholz, Theory of time-dependent rupture in the Earth, *J. Geophys. Res.*, *86*, 6039–6051, 1981.

Debenedetti, P. G., *Metastable Liquids*, Princeton Univ. Press, Princeton, N. J., 1996.

Dietrich, J., A constitutive law for rate of earthquake production and its application to earthquake clustering, *J. Geophys. Res.*, *99*, 2601–2618, 1994.

Dobrovolsky, I. R., S. I. Zubkov, and V. I. Miachkin, Estimation of the size of earthquake preparation zones, *Pure Appl. Geophys.*, *117*, 1025–1044, 1979.

Drossel, B., and F. Schwabl, Self-organized critical forest-fire model, *Phys. Rev. Lett.*, *69*, 1629–1632, 1992.

Ellsworth, W. L., A. G. Lindh, W. H. Prescott, and D. G. Herd, The 1906 San Francisco earthquake and the seismic cycle, in *Earthquake Prediction: An International Review*, *Maurice Ewing Ser.*, vol. 4, edited by D. W. Simpson and P. G. Richards, pp. 126–140, AGU, Washington, D. C., 1981.

Eneva, M., and Y. Ben-Zion, Application of pattern recognition to earthquake catalogs generated by model of segmented fault systems in three-dimensional elastic solids, *J. Geophys. Res.*, *102*, 24,513–24,528, 1997a.

Eneva, M., and Y. Ben-Zion, Techniques and parameters to analyze seismicity patterns associated with large earthquakes, *J. Geophys. Res.*, *102*, 17,785–17,795, 1997b.

Ferguson, C. D., W. Klein, and J. B. Rundle, Spinodals, scaling and ergodicity in a model of an earthquake fault with long-range stress transfer, *Phys. Rev. E*, *60*, 1359–1373, 1999.

Fisher, D. S., K. Dahmen, S. Ramanathan, and Y. Ben-Zion, Statistics of earthquakes in simple models of heterogeneous faults, *Phys. Rev. Lett.*, *78*, 4885–4888, 1997.

Freund, L. B., *Dynamic Fracture Mechanics*, Cambridge Univ. Press, New York, 1990.

Frohlich, C., and S. D. Davis, Single-link cluster analysis as a method to evaluate spatial and temporal properties of earthquake catalogues, *Geophys. J. Int.*, *100*, 19–32, 1990.

Frohlich, C., and S. D. Davis, Teleseismic *b* values; or, much ado about 1.0, *J. Geophys. Res.*, *98*, 631–644, 1993.

Fukunaga, K., *Introduction to Statistical Pattern Recognition*, 2nd ed., Academic, San Diego, Calif., 1990.

Gabrielov, A., W. I. Newman, and D. L. Turcotte, An exactly soluble hierarchical clustering model: Inverse cascades, self-similarity, and scaling, *Phys. Rev. E*, *60*, 5293–5300, 1999.

Giering, R., and T. Kaminski, Recipes for adjoint code construction, *ACM Trans. Math. Software*, *24*, 437–474, 1998.

Gluzman, S., and D. Sornette, Self-consistent theory of rupture by progressive diffuse damage, *Phys. Rev. E*, *63*, 066129, doi:10.1103/PhysRevE.63.066129, 2001.

Goltz, C., and M. Bose, Configurational entropy of critical earthquake populations, *Geophys. Res. Lett.*, *29*, 51–54, 2002.

Gross, S., and J. B. Rundle, A systematic test of time-to-failure analysis, *Geophys. J. Int.*, *133*, 57–64, 1998.

Guarino, A., A. Garcimartin, and S. Ciliberto, An experimental test of the critical behavior of fracture precursors, *Eur. Phys. J. B*, *6*, 13–24, 1998.

Guarino, A., S. Ciliberto, and A. Garcimartin, Failure time and microcrack nucleation, *Europhys. Lett.*, *47*(4), 456–461, 1999.

Gunton, J. D., and M. Droz, *Introduction to the Theory of Metastable and Unstable States, Lect. Notes Phys.*, vol. 183, Springer-Verlag, New York, 1983.

Gunton, J. D., M. San Miguel, and P. S. Sahni, The dynamics of first order phase transitions, in *Phase Transitions and Critical Phenomena*, vol. 8, edited by C. Domb and J. L. Lebowitz, pp. 269–482, Academic, San Diego, Calif., 1973.

Gutenberg, B., and C. F. Richter, *Seismicity of the Earth and Associated Phenomena*, Princeton Univ. Press, Princeton, N. J., 1954.

Haken, H., *Synergetics, An Introduction*, 3rd ed., Springer-Verlag, New York, 1983.

Helmstetter, A., and D. Sornette, Subcritical and supercritical regimes in epidemic models of earthquake aftershocks, *J. Geophys. Res.*, *107*(B10), 2237, doi:10.1029/2001JB001580, 2002a.

Helmstetter, A., and D. Sornette, Diffusion of epicenters of earthquake afershocks, Omori's law, and generalized continuous-time random walk models, *Phys. Rev. E*, *66*, 061104, doi:1103/PhysRevE.66.061104, 2002b.

Helmstetter, A., D. Sornette, and J. R. Grasso, Mainshocks are aftershocks of conditional foreshocks: How do foreshock statistical properties emerge from aftershock laws, *J. Geophys. Res.*, *108*(B1), 2046, doi:10.1029/2002JB001991, 2003.

Hill, D. P., et al., Seismicity remotely triggered by the magnitude 7.3 Landers, California, earthquake, *Science*, *260*, 1617–1623, 1993.

Holmes, P., J. L. Lumley, and G. Berkooz, *Turbulence, Coherent Structures, Dynamical Systems, and Symmetry*, Cambridge Univ. Press, New York, 1996.

Huang, J., and D. L. Turcotte, Are earthquakes an example of deterministic chaos?, *Geophys. Res. Lett.*, *17*, 223–226, 1990.

Huang, J., G. Narkounskaia, and D. L. Turcotte, A cellular-automata, slider-block model for earthquakes II. Demonstration of self-organized criticality for a 2-D system, *Geophys. J. Int.*, *111*, 259–269, 1992.

Jaumé, S. C, Changes in earthquake size-frequency distributions underlying accelerating seismic moment/energy release, in *Geocomplexity and the Physics of Earthquakes*, *Geophys. Monogr. Ser.*, vol. 120, edited by J. B. Rundle, D. L. Turcotte, and W. Klein, pp. 199–210, AGU, Washington, D. C., 2000.

Jaumé, S. C., and L. R. Sykes, Evolving towards a critical point: A review of accelerating seismic moment/energy release prior to large earthquakes, *Pure Appl. Geophys.*, *155*, 279–306, 1999.

Jensen, H. J., *Self-Organized Criticality: Emergent Behavior in Physical and Biological Sciences*, Cambridge Univ. Press, New York, 1998.

Johansen, A., and D. Sornette, Critical ruptures, *Eur. Phys. J. B*, *18*, 163–181, 2000.

Kachanov, L. M., *Introduction to Continuum Damage Mechanics*, Martinus Nijhoff, Zoetermeer, Netherlands, 1986.

Kagan, Y. Y., and D. D. Jackson, Probabilistic forecasting of earthquakes, *Geophys. J. Int.*, *143*, 438–453, 2000.

Kagan, Y. Y., and L. Knopoff, Stochastic synthesis of earthquake catalogs, *J. Geophys. Res.*, *86*, 2853–2862, 1981.

Kagan, Y. Y., and L. Knopoff, Statistical short-term earthquake prediction, *Science*, *236*, 1467–1563, 1987.

Kanninen, M. F., and C. H. Popelar, *Advanced Fracture Mechanics*, Oxford Univ. Press, New York, 1985.

Keilis-Borok, V. I., The lithosphere of the Earth as a nonlinear system with implications for earthquake prediction, *Rev. Geophys.*, *28*, 19–34, 1990.

Keilis-Borok, V. I., and V. G. Kossobokov, Premonitory activation of earthquake flow: Algorithm M8, *Phys. Earth Planet. Inter.*, *61*, 73–83, 1990.

Keilis-Borok, V. I., and I. M. Rotwain, Diagnosis of time of increased probability of strong earthquakes in different regions of the world: Algorithm CN, *Phys. Earth Planet. Inter.*, *61*, 57–72, 1990.

Keilis-Borok, V. I., and A. A. Soloviev (Eds.), *Nonlinear Dynamics of the Lithosphere and Earthquake Prediction*, Springer-Verlag, New York, 2003.

Klein, W., and F. Leyvraz, Crystalline nucleation in deeply quenched liquids, *Phys. Rev. Lett.*, *57*, 2845–2848, 1986.

Klein, W., and C. Unger, Psuedospinodals, spinodals, and nucleation, *Phys. Rev. B*, *28*, 445–448, 1983.

Klein, W., C. Ferguson, and J. B. Rundle, Spinodals and scaling in slider block models, in *Reduction and Predictability of Natural Hazards*, *Santa Fe Inst. Ser. Sci. Complexity*, vol. XXV, edited by J. B. Rundle, D. L. Turcotte, and W. Klein, pp. 223–242, Addison-Wesley-Longman, Reading, Mass., 1996.

Klein, W., J. B. Rundle, and C. D. Ferguson, Scaling and nucleation in models of earthquake faults, *Phys. Rev. Lett.*, *78*, 3793–3796, 1997.

Klein, W., M. Anghel, C. D. Ferguson, J. B. Rundle, and J. S. S. Martins, Statistical analysis of a model for earthquake faults with long-range stress transfer, in *Geocomplexity and the Physics of Earthquakes*, edited by J. B. Rundle, D. L. Turcotte, and W. Klein, *Geophys. Monogr. Ser.*, vol. 120, pp. 43–72, AGU, Washington, D. C., 2000.

Knopoff, L., T. Levshina, V. I. Keilis-Borok, and C. Mattoni, Increased long-range intermediate-magnitude earthquake activity prior to strong earthquakes in California. *J. Geophys. Res.*, *101*, 5779–5796, 1996.

Krajcinovic, D., *Damage Mechanics*, Elsevier Sci., New York, 1996.

Kun, F., and H. J. Herrmann, Transition from damage to fragmentation in collision of solids, *Phys. Rev. E*, *59*, 2623–2632, 1999.

Lay, T., and T. C. Wallace, *Modern Global Seismology*, Academic, San Diego, Calif., 1995.

Lermusiaux, P. F. J., and A. R. Robinson, Data assimilation via error subspace statistical estimation, part I, Theory and schemes, *Mon. Weather Rev.*, *127*, 1385–1407, 1999.

Lorenz, E. N., Deterministic nonperiodic flow, *J. Atmos. Sci.*, *20*, 130–141, 1963.

Lyakhovsky, V., Y. Ben-Zion, and A. Agnon, Distributed damage, faulting and friction, *J. Geophys. Res.*, *102*, 27,635–27,649, 1997.

Ma, S.-K., *Modern Theory of Critical Phenomena*, Benjamin-Cummings, Menlo Park, Calif., 1976.

Main, I. G., Statistical physics, seismogenesis, and seismic hazard, *Rev. Geophys.*, *34*, 433–462, 1996.

Main, I. G., Applicability of time-to-failure analysis to accelerated strain before earthquakes and volcanic eruptions, *Geophys. J. Int.*, *139*, F1–F6, 1999.

Main, I. G., A damage mechanics model for power-law creep and earthquake aftershock and foreshock sequences, *Geophys. J. Int.*, *142*, 151–161, 2000.

Malamud, B. D., G. Morein, and D. L. Turcotte, Forest fires: An example of self-organized critical behavior, *Science*, *281*, 1840–1842, 1998.

Matsu'ura, M., K. Nakajima, and P. Mora (Eds.), *Proceedings of the 2nd ACES Workshop*, Asia Pac. Econ. Coop. for Earthquake Simul., Brisbane, Queensland, Australia, 2001.

May, R. M., Simple mathematical models with very complicated dynamics, *Nature*, *261*, 459–467, 1976.

Miller, S. A., Y. Ben-Zion, and J. P. Burg, A three-dimensional fluid-controlled earthquake model: Behavior and implications, *J. Geophys. Res.*, *104*, 10,621–10,638, 1999.

Mogi, K., Study of elastic shocks caused by the fracture of heterogeneous materials and its relations to earthquake phenomena, *Bull. Earthquake Res. Inst. Univ. Tokyo*, *40*, 125–173, 1962.

Molchan, G. M., and Y. Y. Kagan, Earthquake prediction and its optimization, *J. Geophys. Res.*, *97*, 4823–4838, 1992.

Mora, P. (Ed.), *Proceedings of the 1st ACES Workshop*, Asia Pac. Econ. Coop. for Earthquake Simul., Brisbane, Queens-

land, Australia, 1999.
Morein, G., and D. L. Turcotte, Localized vibrations in slider-block models, *Phys. Rev. E*, *57*, 5126–5134, 1998.
Morein, G., D. L. Turcotte, and A. Gabrielov, On the statistical mechanics of distributed seismicity, *Geophys. J. Int.*, *131*, 552–558, 1997.
Mori, H., and Y. Kuramoto, *Dissipative Structures and Chaos*, Springer-Verlag, New York, 1997.
Nakatani, M., Conceptual and physical clarification of rate and state friction: Frictional sliding as a thermally activated rheology, *J. Geophys. Res.*, *106*, 13,347–13,380, 2001.
Newman, W. I., and S. L. Phoenix, Time dependent fiber-bundles with local load sharing, *Phys. Rev. E*, *63*, 021507, doi:10.1103/PhysRevE.63.021507, 2001.
Nijhout, H. F., L. Nadel, and D. L. Stein (Eds.), *Pattern Formation in the Physical and Biological Sciences*, Addison-Wesley-Longman, Reading, Mass., 1997.
Ogata, Y., Statistical models for earthquake occurrence and residual analysis for point processes, *JASA J. Am. Stat. Assoc.*, *83*, 9–27, 1988.
Otani, H., S. L. Phoenix, and P. Petrina, Matrix effects on lifetime statistics for carbon fibre-epoxy microcomposites in creep rupture, *J. Mater. Sci.*, *26*, 1955–1970, 1991.
Palmer, T., A weather eye on unpredictability, in *Exploring Chaos, A Guide to the New Science of Disorder*, edited by N. Hall, pp. 69–81, W. W. Norton, New York, 1991.
Preisendorfer, R. W., and C. D. Mobley, *Principal Component Analysis in Meteorology and Oceanography*, Elsevier Sci., New York, 1988.
Rabinowicz, E., *Friction and Wear of Materials*, 2nd ed., John Wiley, Hoboken, N. J., 1995.
Ray, T. S., and W. Klein, Nucleation near the spinodal in long-range Ising models, *J. Stat. Phys.*, *61*, 891–902, 1990.
Read, P. L., Application of chaos to meteorology and climate, in *The Nature of Chaos*, edited by T. Mullin, pp. 222–260, Oxford Sci., Oxford, U. K., 1993.
Robertson, M. C., C. G. Sammis, M. Sahimi, and A. J. Martin, Fractal analysis of three-dimensional spatial distributions of earthquakes with a percolation interpretation, *J. Geophys. Res.*, *100*, 609–620, 1995.
Robinson, R., A test of the precursory accelerating moment release model on some recent New Zealand earthquakes, *Geophys. J. Int.*, *140*, 568–576, 2000.
Rundle, J. B., A physical model for earthquakes: 3. Thermodynamic approach and its relation to nonclassical theories of nucleation, *J. Geophys. Res.*, *94*, 2839–2855, 1989.
Rundle, J. B., and D. D. Jackson, Numerical simulation of earthquake sequences, *Bull. Seismol. Soc. Am.*, *67*, 1363–1377, 1977.
Rundle, J. B., and W. Klein, Nonclassical nucleation and growth of cohesive tensile cracks, *Phys. Rev. Lett.*, *63*, 171–174, 1989.
Rundle, J. B., and W. Klein, Scaling and critical phenomena in a cellular automaton slider block model for earthquakes, *J. Stat. Phys.*, *72*, 405–412, 1993.
Rundle, J. B., and W. Klein, New ideas about the physics of earthquakes, *U.S. Natl. Rep. Int. Union Geod. Geophys. 1991–1994, Rev. Geophys.*, *33*, 283–286, 1995a.
Rundle, J. B., and W. Klein, Dynamical segmentation and rupture patterns in a "toy" slider-block model for earthquakes, *J. Nonlinear Proc. Geophys.*, *2*, 61–81, 1995b.
Rundle, J. B., W. Klein, S. Gross, and D. L. Turcotte, Boltzmann fluctuations in numerical simulations of nonequilibrium threshold systems, *Phys. Rev. Lett.*, *75*, 1658–1661, 1995.
Rundle, J. B., W. Klein, and S. Gross, Dynamics of a traveling density wave model for earthquakes, *Phys. Rev. Lett.*, *76*, 4285–4288, 1996.
Rundle, J. B., W. Klein, S. Gross, and C. D. Ferguson, The traveling density wave model for earthquakes and driven threshold systems, *Phys. Rev. E*, *56*, 293–302, 1997a.
Rundle, J. B., S. Gross, W. Klein, C. D. Ferguson, and D. L. Turcotte, The statistical mechanics of earthquakes, *Tectonophysics*, *277*, 147–164, 1997b.
Rundle, J. B., E. Preston, S. McGinnis, and W. Klein, Why earthquakes stop: Growth and arrest in stochastic fields, *Phys. Rev. Lett.*, *80*, 5698–5701, 1998.
Rundle, J. B., W. Klein, and S. Gross, Physical basis for statistical patterns in complex earthquake populations: Models, predictions and tests, *Pure Appl. Geophys.*, *155*, 575–607, 1999.
Rundle, J. B., W. Klein, D. L. Turcotte, and B. D. Malamud, Precursory seismic activation and critical point phenomena, *Pure Appl. Geophys.*, *157*, 2165–2182, 2000a.
Rundle, J. B., D. L. Turcotte, and W. Klein (Eds.), *Geocomplexity and the Physics of Earthquakes*, *Geophys. Monogr. Ser.*, vol. 120, AGU, Washington, D. C., 2000b.
Rundle, J. B., W. Klein, and K. F. Tiampo, Linear pattern dynamics in nonlinear threshold systems, *Phys. Rev. E*, *61*, 2418–2431, 2000c.
Rundle, J. B., W. Klein, K. F. Tiampo, and S. J. Gross, Dynamics of seismicity patterns in systems of earthquake faults, in *Geocomplexity and the Physics of Earthquakes*, *Geophys. Monogr. Ser.*, vol. 120, edited by J. B. Rundle, D. L. Turcotte, and W. Klein, pp. 127–146, AGU, Washington D. C., 2000d.
Rundle, P. B., J. B. Rundle, K. F. Tiampo, J. Sá Martins, S. McGinnis, and W. Klein, Nonlinear network dynamics on earthquake fault systems, *Phys. Rev. Lett.*, *87*, 148501, doi: 10.1103/PhysRevLett.87.148501, 2001.
Rundle, J. B., K. F. Tiampo, W. Klein, and J. S. Sá Martins, Self-organization in leaky threshold systems: The influence of near-mean field dynamics and its implications for earthquakes, neurobiology, and forecasting, *Proc. Natl. Acad. Sci. U. S. A.*, *99*, suppl., 2514–2521, 2002.
Saleur, H., C. G. Sammis, and D. Sornette, Renormalization group theory of earthquakes, *Nonlinear Proc. Geophys.*, *3*, 102–109, 1996a.
Saleur, H., C. G. Sammis, and D. Sornette, Discrete scale invariance, complex fractal dimensions, and log-periodic fluctuations in seismicity, *J. Geophys. Res.*, *101*, 17,661–17,677, 1996b.
Sammis, C. G., and R. L. Biegel, Fractals, fault-gauge, and friction, *Pure Appl. Geophys.*, *131*, 255–271, 1989.
Sammis, C. G., and D. Sornette, Positive feedback, memory, and the predictability of earthquakes, *Proc. Natl. Acad. Sci. U. S. A.*, *99*, 2501–2508, 2002.
Sammis, C. G., and S. J. Steacy, Fractal fragmentation in crustal shear zones, in *Fractals in the Earth Sciences*, edited by C. Barton and P. R. La Pointe, pp. 179–204, Plenum, New York, 1995.
Sammis, C. G., R. H. Osborne, J. L. Anderson, M. Banerdt, and P. White, Self-similar cataclasis in the formation of fault gauge, *Pure Appl. Geophys.*, *124*, 53–78, 1986.
Sammis, C. G., G. King, and R. L. Biegel, The kinematics of gouge deformation, *Pure Appl. Geophys.*, *125*, 777–812, 1987.
Sammis, C. G., D. Sornette, and H. Saleur, Complexity and earthquake forecasting, in *Reduction and Predictability of Natural Hazards*, *Santa Fe Inst. Ser. Sci. Complexity*, vol. XXV, edited by J. B. Rundle, D. L. Turcotte, and W. Klein, pp. 143–156, Addison-Wesley-Longman, Reading, Mass., 1996.
Scholz, C. H., Earthquakes and faulting: Self-organized critical phenomena with a characteristic dimension, in *Spontaneous Formation of Space Time Structure and Criticality*, edited by T. Riste and D. Sherrington, pp. 41–56, Kluwer Acad., Norwell, Mass., 1991.

Scholz, C. H., *The Mechanics of Earthquakes and Faulting*, 2nd ed., Cambridge Univ. Press, New York, 2002.

Schwartz, D., and K. Coppersmith, Fault behavior and characteristic earthquakes: Examples from the Wasatch and San Andreas fault zones, *J. Geophys. Res.*, *89*, 5681–5698, 1984.

Selinger, R. L. B., Z. G. Wang, W. M. Gelbart, and A. Ben-Shaul, Statistical-thermodynamic approach to fracture, *Phys. Rev. A*, *43*, 4396–4400, 1991.

Shaw, B. E., Generalized Omori law for aftershocks and foreshocks from a simple dynamics, *Geophys. Res. Lett.*, *20*, 907–910, 1993.

Shcherbakov, R., and D. L. Turcotte, Damage and self-similarity in fracture, *Theor. Appl. Frac. Mech.*, *39*, 245–258, 2003a.

Shcherbakov, R., and D. L. Turcotte, A damage mechanics model for aftershocks, *Pure Appl. Geophys.*, in press, 2003b.

Smalley, R. F., D. L. Turcotte, and S. A. Solla, A renormalization-group approach to the stick-slip behavior of faults, *J. Geophys. Res.*, *90*, 1894–1900, 1985.

Smith, R. L., and S. L. Phoenix, Asymptotic distributions for the failure of fibrous materials under series-parallel structure and equal load-sharing, *J. Appl. Mech.*, *48*, 75–82, 1981.

Sornette, D., Discrete-scale invariance and complex dimensions, *Phys. Rep.*, *297*, 239–270, 1998.

Sornette, D., and J. V. Andersen, Scaling with respect to disorder in time-to-failure, *Eur. Phys. J. B*, *1*, 353–357, 1998.

Sornette, D., and C. G. Sammis, Complex critical exponents form renormalization group theory of earthquakes: Implications for earthquakes predictions, *J. Phys. I*, *5*, 607–619, 1995.

Stanley, H. E., *Introduction to Phase Transitions and Critical Phenomena*, Clarendon, Oxford, U. K., 1971.

Stein, R. S., The role of stress transfer in earthquake occurence, *Nature*, *402*, 605–609, 1999.

Sykes, L. R., and S. C. Jaumé, Seismic activity on neighbouring faults as a long-term precursor to large earthquakes in the San Francisco Bay area, *Nature*, *348*, 595–599, 1990.

Tiampo, K. F., J. B. Rundle, S. McGinnis, S. J. Gross, and W. Klein, Observation of systematic variations in non-local seismicity patterns from southern California, in *Geocomplexity and the Physics of Earthquakes*, *Geophys. Monogr. Ser.*, vol. 120, edited by J. B. Rundle, D. L. Turcotte, and W. Klein, pp. 211–218, AGU, Washington D. C., 2000.

Tiampo, K. F., J. B. Rundle, S. McGinnis, S. J. Gross, and W. Klein, Mean field threshold systems and earthquakes: An application to earthquake fault systems, *Europhys. Lett.*, *60*(3), 481–487, 2002a.

Tiampo, K. F., J. B. Rundle, S. McGinnis, and W. Klein, Pattern dynamics and forecast methods in seismically active regions, *Pure Appl. Geophys.*, *159*, 2429–2467, 2002b.

Tiampo, K. F., J. B. Rundle, S. McGinnis, and S. J. Gross, Eigenpatterns in southern California seismically, *J. Geophys. Res.*, *107*(B12), 2354, doi:10.1029/2001JB000562, 2002c.

Turcotte, D. L., A fractal approach to probabilistic seismic hazard assessment, *Tectonophysics*, *167*, 171–177, 1989.

Turcotte, D. L., Earthquake prediction, *Annu. Rev. Earth. Planet. Sci.*, *19*, 263–281, 1991.

Turcotte, D. L., *Fractals and Chaos in Geology and Geophysics*, 2nd ed., Cambridge Univ. Press, New York, 1997.

Turcotte, D. L., Self-organized criticality, *Rep. Prog. Phys.*, *62*, 1377–1429, 1999.

Turcotte, D. L., W. I. Newman, and R. Shcherbakov, Micro- and macro-scopic models of rock fracture, *Geophys. J. Int.*, *152*, 718–728, 2003.

Varnes, D. J., Predicting earthquakes by analyzing accelerating precursory seismic activity, *Pure Appl. Geophys.*, *130*, 661–686, 1989.

Varnes, D. J., and C. G. Bufe, The cyclic and fractal seismic series preceding on m_b = 4.8 earthquake on 1980 February 14 near the Virgin Islands, *Geophys. J. Int.*, *124*, 149–158, 1996.

Vere-Jones, D., R. Robinson, and W. Yang, Remarks on the accelerated moment release model: Problems of model formulation, simulation, and estimation, *Geophys. J. Int.*, *144*, 517–531, 2001.

Wu, H. F., S. L. Phoenix, and P. Schwartz, Temperature dependence of lifetime statistics for single Kevlar 49 filaments in creep-rupture, *J. Mater. Sci.*, *23*, 1851–1860, 1988.

Zapperi, S., P. Ray, H. E. Stanley, and A. Vespignani, First-order transition in the breakdown of disordered media, *Phys. Rev. Lett.*, *78*, 1408–1411, 1997.

Zapperi, S., P. Ray, H. E. Stanley, and A. Vespignani, Avalanches in breakdown and fracture processes, *Phys. Rev. E*, *59*, 5049–5057, 1999.

Zoback, M. L., First- and second-order patterns of stress in the lithosphere: The World Stress Map project, *J. Geophys. Res.*, *97*, 11,703–11,728, 1992.

Zöller, G., and S. Hainzl, Detecting premonitory seismicity patterns based on critical point dynamics, *Nat. Hazards Earth Syst. Sci.*, *1*, 93–98, 2001.

Zöller, G., and S. Hainzl, A systematic spatiotemporal test of the critical point hypothesis for large earthquakes, *Geophys. Res. Lett.*, *29*(1), 1558, doi:10.1029/2002GL014856, 2002.

Zöller, G., S. Hainzl, and J. Kurths, Observation of growing correlation length: An indicator for critical point behavior prior to large earthquakes, *J. Geophys. Res.*, *106*, 2167–2175, 2001.

W. Klein, Department of Physics, Boston University, Boston, MA 02215, USA. (klein@physics.bu.edu)

J. B. Rundle and R. Shcherbakov, Center for Computational Science & Engineering, Department of Physics, University of California, Davis, Davis, CA 95616, USA. (rundle@physics.ucdavis.edu; roshch@physics.ucdavis.edu)

C. Sammis, Department of Geology and Geophysics, University of Southern California, Los Angeles, CA 90089, USA. (sammis@usc.edu)

D. L. Turcotte, Department of Geology, University of California, Davis, One Shields Avenue, Davis, CA 95616, USA. (turcotte@geology.ucdavis.edu)